Arterial Spin Labeling Perfusion of the Brain: Emerging Clinical Applications[1]

Sven Haller, MD, MSc
Greg Zaharchuk, MD, PhD
David L. Thomas, PhD
Karl-Olof Lovblad, MD
Frederik Barkhof, MD
Xavier Golay, PhD

Online SA-CME
See www.rsna.org/education/search/ry

Learning Objectives:

After reading the article and taking the test, the reader will be able to:

- Describe the technical principles of arterial spin labeling
- Discuss the limitations and pitfalls of ASL
- Discuss the role of ASL in neurodegenerative and cerebrovascular disease, arteriovenous malformation, epilepsy, neoplasms, and neurologic disorders
- Discuss the use of ASL to measure cerebrovascular reserve using a vascular challenge

Accreditation and Designation Statement

The RSNA is accredited by the Accreditation Council for Continuing Medical Education (ACCME) to provide continuing medical education for physicians. The RSNA designates this journal-based SA-CME activity for a maximum of 1.0 *AMA PRA Category 1 Credit™*. Physicians should claim only the credit commensurate with the extent of their participation in the activity.

Disclosure Statement

The ACCME requires that the RSNA, as an accredited provider of CME, obtain signed disclosure statements from the authors, editors, and reviewers for this activity. For this journal-based CME activity, author disclosures are listed at the end of this article.

[1] From Affidea Centre Diagnostique Radiologique de Carouge, Clos de la Fonderie 1, 1227 Carouge, Switzerland (S.H.); Dept of Surgical Sciences, Div of Radiology, Uppsala Univ, Sweden (S.H.); Dept of Neuroradiology, Univ Hosp Freiburg, Germany (S.H.); Faculty of Medicine Univ of Geneva, Switzerland (S.H.); Dept of Radiology, Stanford Univ, Stanford, Calif (G.Z.); Univ College London, Inst of Neurology, London, England (D.L.T., X.G.); Dept of Diagnostic and Interventional Neuroradiology, Geneva Univ Hosps,Switzerland (K.O.L.); Dept of Radiology & Nuclear Medicine and PET Research, VU Univ Medical Ctr, Amsterdam, the Netherlands (F.B.); and Insts of Neurology and Healthcare Engineering, Univ College London, England (F.B.). Rec Apr 13, 2015; rev request June 1; rev rec June 14; accepted July 6; final accept July 21. **Address correspondence to** S.H. (e-mail: *sven.haller@gmail.com*).

Supported in part by COST Action BM1103 on ASL in dementia.

Arterial spin labeling (ASL) is a magnetic resonance (MR) imaging technique used to assess cerebral blood flow noninvasively by magnetically labeling inflowing blood. In this article, the main labeling techniques, notably pulsed and pseudocontinuous ASL, as well as emerging clinical applications will be reviewed. In dementia, the pattern of hypoperfusion on ASL images closely matches the established patterns of hypometabolism on fluorine 18 fluorodeoxyglucose (FDG) positron emission tomography (PET) images due to the close coupling of perfusion and metabolism in the brain. This suggests that ASL might be considered as an alternative for FDG, reserving PET to be used for the molecular disease-specific amyloid and tau tracers. In stroke, ASL can be used to assess perfusion alterations both in the acute and the chronic phase. In arteriovenous malformations and dural arteriovenous fistulas, ASL is very sensitive to detect even small degrees of shunting. In epilepsy, ASL can be used to assess the epileptogenic focus, both in peri- and interictal period. In neoplasms, ASL is of particular interest in cases in which gadolinium-based perfusion is contraindicated (eg, allergy, renal impairment) and holds promise in differentiating tumor progression from benign causes of enhancement. Finally, various neurologic and psychiatric diseases including mild traumatic brain injury or posttraumatic stress disorder display alterations on ASL images in the absence of visualized structural changes. In the final part, current limitations and future developments of ASL techniques to improve clinical applicability, such as multiple inversion time ASL sequences to assess alterations of transit time, reproducibility and quantification of cerebral blood flow, and to measure cerebrovascular reserve, will be reviewed.

Online supplemental material is available for this article.

Arterial spin labeling (ASL) is a magnetic resonance (MR) imaging technique that enables the measurement of brain perfusion noninvasively at the tissue level. Benefiting from the contrast of inflowing magnetically labeled blood, ASL obviates an exogenous contrast agent. Although the principle of ASL was introduced in early 1990s (1–3) and is feasible on low-field-strength MR systems, ASL greatly benefits from the improved signal-to-noise ratio (SNR) of modern high-field-strength MR imaging systems (4). The increasing availability of 3-T imagers, as well as the development of improved pulse sequences and multichannel receiver array coils, has led to a rapidly growing interest in ASL within the past few years, paving the way for widespread application in neurologic and psychiatric disorders. The current review will start by briefly summarizing the essential technical requirements and then discuss in more detail emerging clinical applications of ASL (such as in dementia, stroke, vascular malformations, epilepsy, tumors, and psychiatry) and concludes with a critical review of the current limitations and future perspectives of brain ASL imaging.

Essentials

- Due to the close link between brain metabolism and perfusion, patterns of fluorine 18 fluorodeoxyglucose PET closely resemble those of arterial spin labeling (ASL).
- ASL complements structural information of standard MR imaging in neurocognitive decline and may allow early diagnosis of dementia.
- ASL may depict mismatch perfusion in acute stroke and help identify tissue at risk in chronic cerebrovascular disease.
- ASL may depict arteriovenous shunting in arteriovenous malformation and fistulas.
- ASL may be used to localize the epileptogenic focus in seizure disorders.
- In neoplasms, ASL may replace standard gadolinium-enhanced dynamic susceptibility contrast-enhanced imaging, notably in patients with allergies or renal insufficiency or in children.
- ASL may help detect subtle functional changes in psychiatric disorders such as posttraumatic stress disorder or mild traumatic brain injury, where standard structural MR imaging typically provides no detectable anomaly.
- Emerging new applications of ASL include superselective ASL to map vascular territories and cerebrovascular reserve imaging.

Essential Technical Considerations

Basic Concepts of ASL

ASL is based on the principle of magnetically labeling inflowing arterial blood protons prior to their entry into the tissue of interest. As such, it can be viewed as a tracer technique (5,6), with water acting as the natural endogenous tracer to estimate tissue perfusion. The label is created by applying radiofrequency pulses to invert the bulk magnetization of the blood water protons. Images are acquired after the labeling and inflow period by using rapid acquisition techniques such as echo-planar imaging, gradient- and spin-echo imaging (GRASE), or three-dimensional fast spin-echo imaging using a stack-of-spirals approach (7–9). A pair of images is always acquired: a labeled image, in which the blood water magnetization is inverted, and a control image, in which the blood water magnetization is not inverted. The signal difference between labeled and control images is proportional to the amount of magnetization inverted and delivered to the tissue. If all the labeled blood has arrived at the imaging voxel at the time of image acquisition, the signal difference will be proportional to cerebral blood flow (CBF). The current main implementations of ASL are pulsed and pseudocontinuous labeling.

Pulsed ASL

In pulsed ASL (PASL), the arterial blood water is labeled by using a short adiabatic inversion pulse. The labeling pulses are on the order of approximately 10 msec and designed to invert the blood water instantaneously in a particular region, typically located inferior to the brain (Fig 1a). After labeling, a postlabel delay period is required (also known as the inflow time for PASL), during which time the inverted blood moves from the labeling region into the brain, losing gradually its label through longitudinal T1 relaxation. For this reason, PASL is intrinsically a lower SNR technique than pseudocontinuous ASL (PCASL). The control acquisition for PASL consists of applying a radiofrequency pulse with equivalent power to the labeling pulse but which has a net zero effect on the blood water magnetization in the labeling region.

PCASL Technique

In PCASL, a long labeling period (1–2 seconds) is made up of a train of very short (≈1 msec) pulses (9). This train of short pulses is designed to invert the inflowing blood magnetization in an adiabatic or pseudo steady-state manner (Fig 1b). It is useful to think of the blood being continuously inverted as it flows through a "labeling plane" in the inferior-superior direction. If the phase of every second pulse in the PCASL pulse train is shifted by 180°, the flowing blood water is minimally perturbed and thus enables acquisition of nonlabeled control images. PCASL has

Published online
10.1148/radiol.2016150789 **Content code:** NR

Radiology 2016; 281:337–356

Abbreviations:
AD = Alzheimer disease
ASL = arterial spin labeling
BOLD = blood oxygen level dependent
CBF = cerebral blood flow
DSC = dynamic susceptibility contrast
FDG = fluorine 18 fluorodeoxyglucose
PASL = pulsed ASL
PCASL = pseudocontinuous ASL
SNR = signal-to-noise ratio

Conflicts of interest are listed at the end of this article.

Figure 1

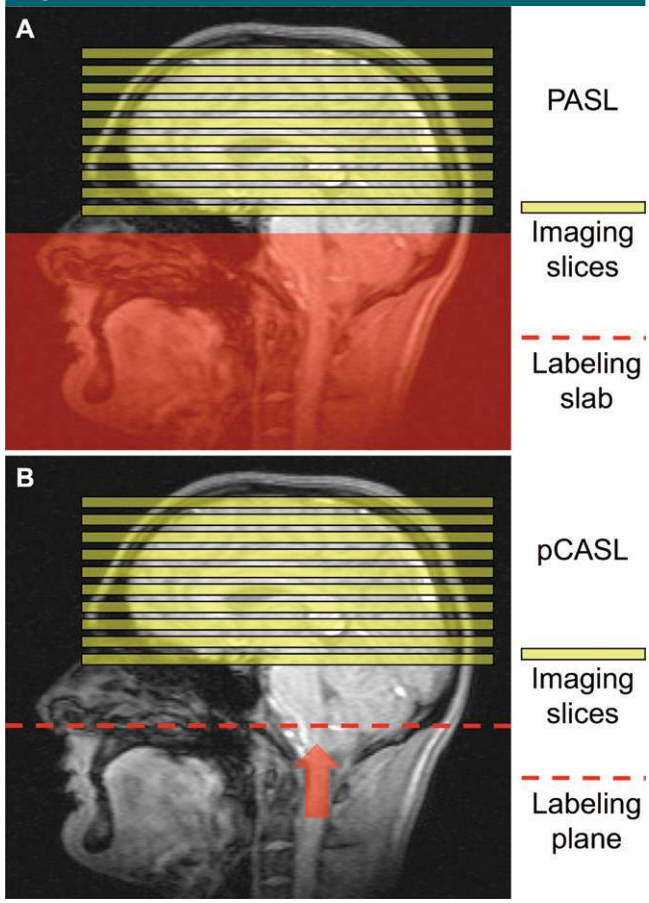

Figure 1: ASL labeling schemes. *A,* In PASL, an inversion slab is placed proximal to the imaging volume to label blood in the arterial feeding vessels supplying the brain. The pulse is short (~10 msec) and all the blood is inverted simultaneously. *B,* In PCASL, the inflowing arterial blood is continuously inverted as it flows through the labeling plane by means of a process known as flow-induced adiabatic inversion. The PCASL labeling pulse train is typically applied for a period of approximately 1–2 seconds.

recently been adopted as the labeling method of choice for clinical imaging, due to its ease of implementation and high SNR (10).

Pros and Cons: PASL versus PCASL

The main advantage of PCASL over PASL is its higher SNR—a substantial benefit in a technique that is intrinsically SNR limited. The reason for this can be understood by considering the degree of labeling of the arterial blood as it arrives at the tissue and how this changes during the inflow time and/or postlabel delay (Fig 2). For PASL, a slab of arterial blood is inverted at inflow time of 0, and subsequently undergoes T1 relaxation during the inflow time. For PCASL, the arterial blood is continuously inverted as it passes through the labeling plane, which means that all the blood has the same amount of T1 decay when it arrives at the tissue, irrespective of when it was labeled. However, the benefits of PCASL are not as large in practice as would be predicted theoretically due to *(a)* the inversion efficiency of the radiofrequency pulses used in PASL, higher than that achieved by using the PCASL flow-induced adiabatic inversion pulse train; *(b)* the sensitivity of the PCASL labeling train to off-resonance effects, which can cause apparent regional hypoperfusion if different feeding arteries are affected differently; and *(c)* the longer arterial arrival times for PCASL for which the labeling plane is required to intersect major feeding arteries with flow in a known direction, generally placed distally to the PASL labeling slab. Consequently, for any given study, it is always worth to consider the specific pros and cons of PCASL and PASL to choose the most appropriate option.

The Critical Importance of the Postlabel Delay Time

An important aspect of all ASL techniques is the introduction of the postlabel delay (or inflow time) between the end of the labeling pulse and the time of image acquisition (11). If the postlabel delay is longer than the longest transit time between the tagging plane and the imaging volume, the ASL signal becomes insensitive to variations in the arterial arrival time, as long as the blood and tissue T1 values are similar (true for gray matter but not for white matter) (11,12). This enables CBF quantification and minimizes the appearance of intravascular signal in the ASL images, yet at the expense of SNR, due to the T1 relaxation of the bolus (T1 of blood is 1600 msec at 3 T). In addition, the choice of postlabel delay depends on the subject's age, with older subjects showing longer arterial arrival times. The recommended postlabel delay for pediatric and adult clinical populations is 1500 msec and 2000 msec, respectively (10).

Alterations of Transit Time: Multi–Inflow-Time ASL

Most clinically available ASL sequences use only a single delay between labeling and image acquisition, based on original values calculated from healthy young adults. In case of proximal vessel occlusion, there is a delayed arrival of blood in the parenchyma, which may falsely suggest a reduced relative CBF as estimated with ASL (Fig 3) (13) and increased ASL signal in the feeding arterial vessels, known as arterial transit artifact (14). Reduced cardiac output, as seen frequently in elderly

Figure 2

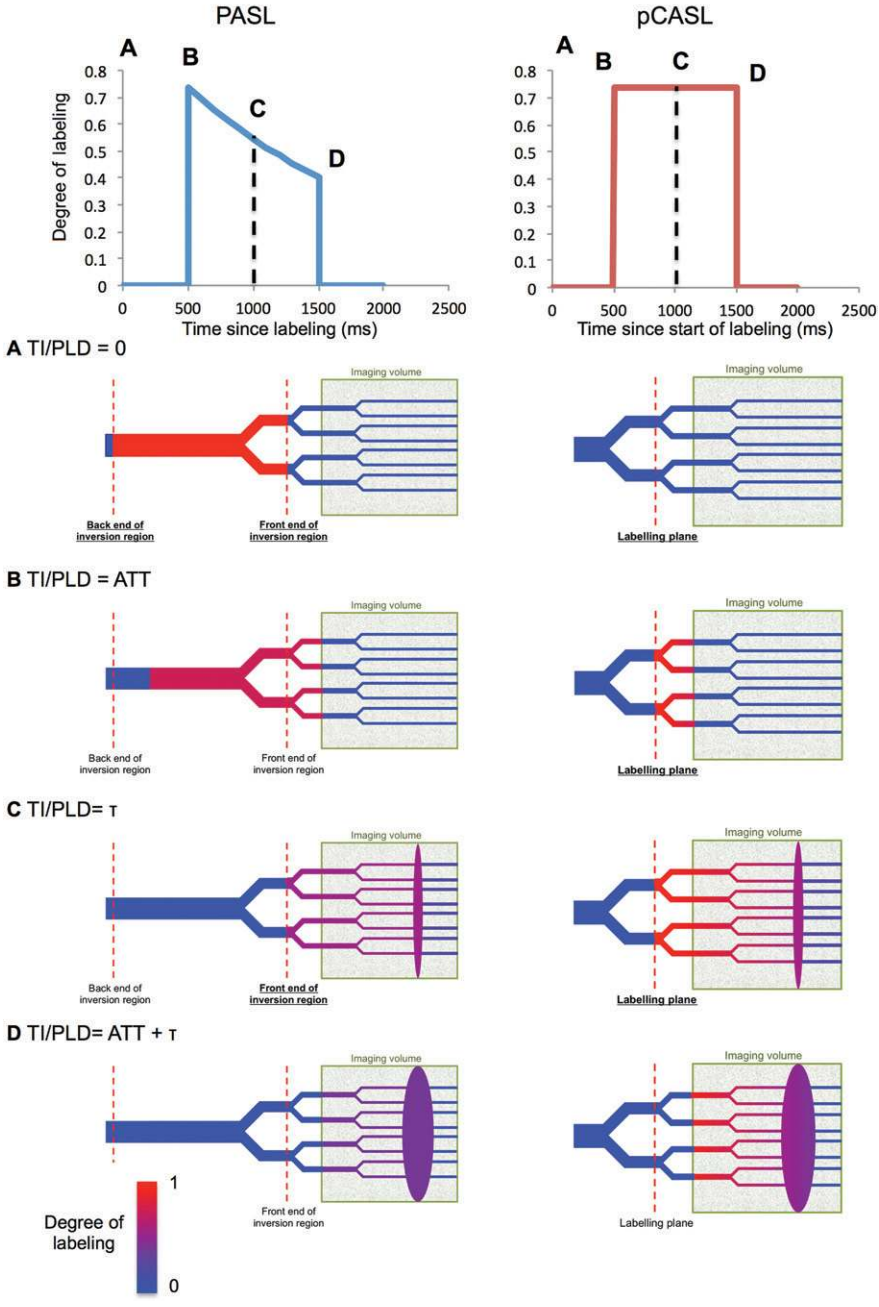

Figure 2: Differences in labeling degree of ASL bolus for PASL (left column) and PCASL (right column). The top row shows the temporal profile of the bolus (1 = fully inverted; 0 = fully relaxed). Since the PASL inversion slab is inverted at a single point in time (t = 0 on this graph), all the inflowing arterial blood undergoes the same amount of T1 recovery at all time points after this. In PCASL, blood is labeled as it flows through the inversion plane and recovers en route to the imaging volume. *A–D* show the degree of labeling remaining at several time points after the start of labeling (t = 0): *A,* t = 0; *B,* t = arterial arrival time *(ATT)*; *C,* t = bolus duration (τ); *D,* t = ATT + τ. Color scale represents the range from fully inverted (red) to fully relaxed (blue). It can be seen that the PCASL labeling process produces a bolus with a higher overall degree of inversion than does the PASL, resulting in a higher intrinsic SNR for PCASL.

populations, leads to similar effects, for example, in the vascular border zone regions (15). The use of multi–inflow-time ASL sequences aims to overcome this methodological shortcoming, but due to the longer imaging times required, they are currently not recommended in daily clinical practice (16,17). Other parameters affecting ASL can be found in the Appendix E1 (online).

ASL in Neurodegenerative Diseases

General Considerations: Coupling of Brain Perfusion and Brain Metabolism

Alzheimer dementia is the most common type of dementia. According to the model of neurodegeneration proposed by Jack et al (18), brain metabolic alterations precede structural abnormalities during cognitive decline in Alzheimer dementia. This explains the considerable interest in the assessment of brain glucose metabolism based on fluorine 18 fluorodeoxyglucose (FDG) positron emission tomography (PET) findings in the work up of dementia. This technique has identified typical patterns of metabolic alterations in various types of dementia. For example, Alzheimer dementia is typically associated with hypometabolism in bilateral parietal and temporal regions sparing the occipital lobe, while dementia with Lewy bodies also has bilateral parietal and temporal and additionally occipital hypometabolism (19). One disadvantage of FDG PET is that the alterations in blood glucose metabolism are not specific for a given disease. This has led to the development of disease-specific tracers of amyloid and tau PET, which were recently introduced for clinical use. As a consequence, there is a need for an alternative technique that might be used as a surrogate marker to replace FDG PET in the work up of dementia. ASL is a very promising alternative technique for two reasons. First, perfusion and metabolism are typically tightly coupled in the brain (20,21). This perfusion-metabolism coupling implies that the known patterns of hypometabolism in FDG PET in dementia can be transferred to patterns of hypoperfusion on ASL MR

Figure 3

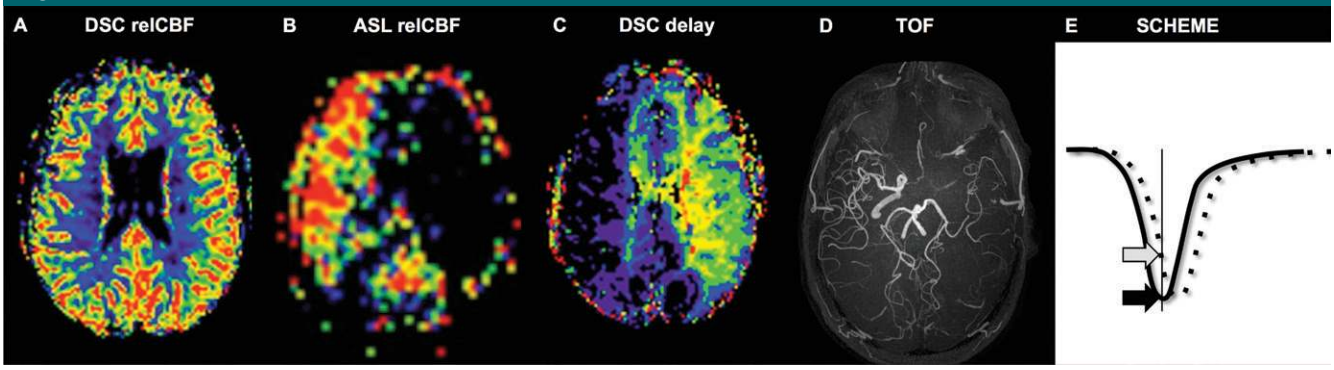

Figure 3: Example of an underestimation of relative CBF *(relCBF)* in ASL due to a proximal vessel stenosis. *A,* The estimated relative CBF based on DSC perfusion is within normal limits. *B,* In contrast, the relative CBF estimated by using a standard single–inflow-time ASL sequence demonstrates marked reduction in the left anterior and middle cerebral artery territories. The origin of this discrepancy is the increased perfusion delay, illustrated on, *C,* DSC-derived delay map, which exactly matches the altered perfusion in ASL due to the presence of a high-grade stenosis of the left internal carotid artery on, *D,* time-of-flight *(TOF)* image. The underlying principle is explained in *E.* The normal perfusion time series of DSC imaging (solid black line) is shifted to the right due to the presence of a proximal vessel stenosis and slower collateral flow (dotted line). DSC imaging acquires an entire time series, this shift in the bolus arrival simply causes a shift of the estimated curve, and the relative CBF can be accurately estimated in DSC. In contrast, a single–inflow-time ASL sequence with a standard inflow time (indicated by the vertical line) will underestimate the true perfusion simply because it is too early with respect to the peak of the perfusion curve.

images. Correspondingly, there is a good correlation between brain perfusion measured by using ASL (22–26) and brain metabolism measured with FDG PET (27–30), for example, in the domain of mild cognitive impairment and Alzheimer dementia. Second, structural MR imaging is routinely performed in many patients during the work up of cognitive decline. Addition of an ASL sequence to the existing MR protocol is minimally demanding for the patient and does not require additional radiation or use of contrast agents, is less costly, and allows for the assessment of brain structure and perfusion in one imaging session. Moreover, if ASL could replace FDG PET, this would enable more disease-specific PET imaging with the newly available amyloid or tau tracers.

Normal Aging

To be able to assess reductions in perfusion measured with ASL in cognitive decline, it is first necessary to understand the evolution of ASL imaging appearances during normal aging. A study of 44 healthy participants from age 4 to 78 years found the highest gray matter perfusion in children (97 mL/100 g/min ± 5 [standard deviation]), which had already decreased in adolescents (79 mL/100 g/min ± 3). After the age of around 20, gray matter perfusion remained rather constant at 58 mL/100 g/min ± 4 until the age of around 80 years (31). Another study of 38 elderly healthy individuals (mean age, 82.2 years ± 3.7) found variable patterns of decreased and increased perfusion (32). Restom and colleagues compared 15 healthy young adults around 25 years of age with 12 healthy elderly control subjects around 75 years of age and found a significantly lower CBF at rest in the elderly (33). Rusinek et al focused on the hippocampus during normal aging from 26 to 92 years of age due to the particular interest of this structure in dementia, and found no significant age or sex effect (34).

More recently, ASL was used in 148 consecutive control subjects and 65 cases with mild cognitive impairment around 76 years of age (35). About half of the control participants developed subtle cognitive decline during follow-up. ASL imaging performed at baseline revealed decreased perfusion in the posterior cingulate cortex in those individuals who later developed subtle cognitive decline, indicating the predictive value of ASL for the earliest form of cognitive decline. Interestingly, the ASL pattern of those deteriorating control subjects was similar to mild cognitive impairment cases, indicating that these individuals were initially able to maintain an intact cognitive status through their cognitive reserve despite already present reductions in CBF.

Alzheimer Disease and Mild Cognitive Impairment

Alzheimer disease (AD) is associated with gray matter volume loss in the mesial temporal and parietal lobes. In earlier stages of the disease, such as mild cognitive impairment or preclinical AD, atrophy can be minimal though metabolic imaging (FDG PET) findings may already be abnormal (18,36).

ASL studies in established AD have consistently shown a reduction in CBF (22–25,30,37,38) in a posterior parietal distribution, including the precuneus, posterior cingulate, angular gyrus, and superior parietal gyrus (25). The ASL pattern is remarkably similar (Fig 4) to the pattern of the hypometabolism seen with FDG PET (39), and both modalities have similar diagnostic performance (38). The information from ASL persists after correction for local gray matter atrophy, illustrating its independent diagnostic value, although uncorrected ASL maps may be preferred in a clinical setting to increase the effect-size. Similar patterns of hypoperfusion

Figure 4

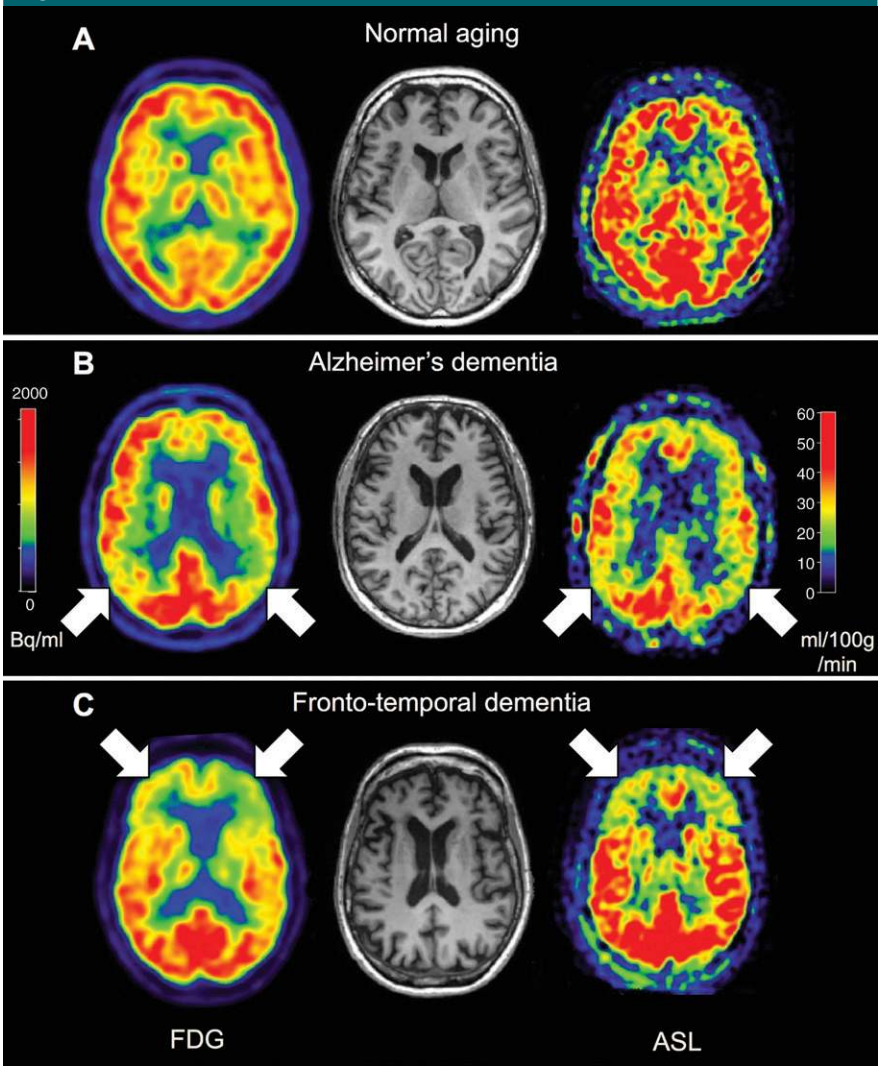

Figure 4: Examples of dementia. Transverse FDG and ASL images of, *A,* a healthy individual (male; age, 57 years; Mini-Mental State Examination [MMSE] score, 30), *B,* patient with AD (male; age, 52 years; MMSE score, 19), and, *C,* patient with frontotemporal lobar dementia (female; age, 53 years; MMSE score, 26). Functional images show predominant prefrontal abnormalities in FTD and parietal abnormalities in AD. Red color reflects normal metabolism and perfusion.

have been observed in subjects with mild cognitive impairment, and preliminary evidence suggests that abnormal perfusion in the precuneus can predict conversion to AD (40), though larger studies are required for confirmation.

Frontotemporal Lobar Dementia, Lewy Body Dementia, and Vascular Dementia

Less is known about the potential of ASL in dementias other than AD. In subjects with frontotemporal lobar dementia, Du et al (30) found right frontal hypoperfusion in 21 patients, similar to FDG PET, while perfusion in parietal regions and posterior cingulate was preserved relative to AD. These findings were confirmed in a study comparing AD and frontotemporal lobar dementia (41), with both ASL and FDG showing a clearly differentiating pattern in frontotemporal lobar dementia compared with AD (Fig 4).

In dementia with Lewy bodies, Taylor et al (42) found posterior hypoperfusion in the posterior cingulate and higher order visual association areas in 15 patients with dementia with Lewy bodies; no comparison with AD was made. In the related Parkinson disease dementia disorder, Le Heron et al (43) found the pattern of posterior hypoperfusion to largely overlap with that in AD patients, hinting at a similar mechanism of neurodegeneration.

Vascular dementia by definition is caused by impaired cerebral perfusion, and widespread decreases in CBF have been found especially in bilateral frontal and parietal areas in subjects with vascular dementia (44,45) and subjects with confluent incidental white matter ischemic changes (46). The pattern overlaps even more with AD in poststroke patients (47), though this may well be due to concomitant (unveiled) Alzheimer pathologic condition. A related point to note here is the limited ability of ASL to measure white matter perfusion. Due to the low perfusion levels and long arterial arrival times in white matter, the SNR of the ASL signal is typically very low, and it is not possible to obtain reliable estimates of CBF unless the acquisition parameters are specifically optimized (48–50).

ASL in Cerebrovascular Disease

Early on, ASL techniques were recognized to be valuable for imaging brain ischemia. Indeed, following the National Institute of Neurologic Disorders and Stroke trial (51) and the development of diffusion imaging, the potential of acquiring brain perfusion images without contrast material was recognized. This allows perfusion imaging in patients with contraindications to intravenous contrast material, such as renal failure, and simplifies the acquisition of quantitative CBF, which is challenging with contrast agent–based perfusion techniques, such as dynamic susceptibility contrast (DSC).

Initial reports of ASL imaging in stroke demonstrated proof of principle but were limited by their inability to image the entire brain (52). Since the widespread use of whole-brain, high-SNR ASL sequences, several studies

Figure 5

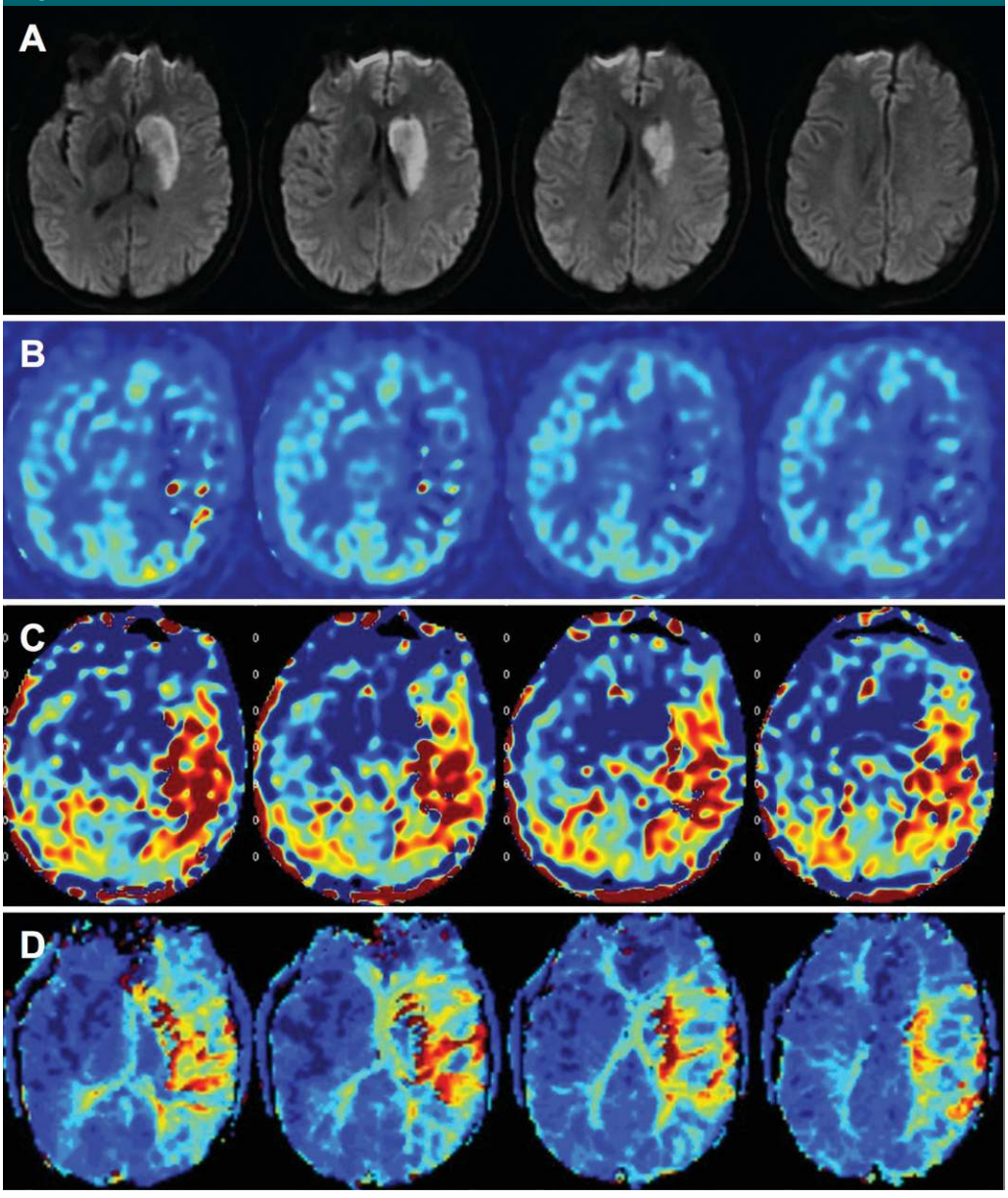

Figure 5: Images in 50-year-old woman presenting with stroke, with 14 hours of right hemiparesis and aphasia, National Institutes of Health Stroke Scale score of 9 at the time of imaging. Patient was later found to have extracranial left internal carotid artery dissection. *A,* Diffusion-weighted images demonstrate irreversibly damaged tissue within the left caudate and putamen. By using a multidelay ASL sequence capable of acquiring both, *B,* CBF and, *C,* arterial transit time images, a larger region of perfusion abnormality is identified. *D,* Conventional DSC images show the region of perfusion abnormality (time to the maximum of the residue function) is concordant with the findings on ASL images.

have shown reasonable concordance of ASL with DSC measures of perfusion deficit, primarily time-based parameters such as the mean transit time and time to peak of the residue function (Fig 5) (53–56). Vessel-selective ASL has the additional advantage of being more sensitive to identify perfusion changes induced by collateral flow (57) in stroke patients. Routine ASL can also show perfusion changes in patients with Moyamoya disease (58). It has also been applied in cases where treatment was initiated on the basis of the presence of collateral flow (59).

The ability of ASL to measure severe hypoperfusion or determine perfusion in regions with prolonged arterial arrival

times remains a critical issue for imaging patients with cerebrovascular disease. In these situations, there can be regions with a lack of ASL signal intensity in the ischemic lesion that render reconstruction of summary maps difficult. However, for the detectability of stroke, ASL techniques have been shown to be at least equivalent to DSC techniques and can be used for a mismatch approach with diffusion-weighted images (54,60). In our experience, it is particularly helpful when ASL shows normal perfusion or hyperperfusion (as is sometimes seen after vessel recanalization), since it eliminates the possibility of a diffusion-perfusion mismatch that would reflect tissue at risk of infarction, thus directly affecting patient treatment.

In patients with known cerebrovascular disease, alternative ASL imaging strategies could be considered, including long-label long-postlabel delay single–time-point ASL and multidelay ASL. The former will mitigate the problem of slow flow not arriving at the tissue bed by the time of imaging, resulting in CBF underestimation. However, differences in the decay of the label when it is within the blood, with its longer T1 compared with tissue, can lead to misinterpretation, with adequate CBF that arrives later than expected appearing hyperintense. Multidelay ASL, in which ASL images with several postlabel delay times are acquired, offers the potential to measure both perfusion and arterial arrival time and use the arrival time information to improve the accuracy of the CBF maps. This addresses some of the problems of long-label long-delay ASL, but at the expense of SNR per unit time. Practically, this means that multidelay ASL images will have reduced spatial resolution unless imaging efficiency is improved or much longer imaging times are accepted. One promising approach to improve the time efficiency of multidelay ASL is Hadamard encoding (61). Hadamard encoding is a method in which blocks of labeling are mixed with blocks of nonlabeling, with different permutations of the labeling and control blocks. This method enables reconstruction of images with different delay times in a more time-efficient manner, leading to higher SNR, particularly for transit time mapping (61,62).

ASL has also been applied to chronic cerebrovascular disease, including carotid stenosis and occlusion (14,63,64) and Moyamoya disease (58,65–68). Such diseases are characterized by near normal CBF, but often striking abnormalities of arterial arrival time, since blood arrives at the parenchyma through alternative pathways. For this reason, many of these studies have availed themselves of multidelay ASL approaches to correct CBF values for arrival time and to map transit time abnormalities directly (Fig 6). Given the relatively long delays, either the use of extremely long-label and postlabel delay times or multidelay ASL is critical for a proper perfusion measurement in these diseases. This being said, even with state-of-the-art techniques, there are a few patients with very severe Moyamoya disease, in which ASL imaging of CBF is practically infeasible because of the extremely circuitous and delayed arrival time of the blood flow due to loss of the magnetic label during the transit between the labeling region and the brain parenchyma.

ASL in Arteriovenous Malformation and Fistula

One unexpected but useful clinical application of ASL imaging is the ability to identify lesions with arteriovenous shunting. Because more than 90% of water is extracted during the first pass through the capillaries, and because the mean dwell time of water molecules once extracted from the vascular into the extravascular space is several minutes, most of the labeled water decays within the brain parenchyma and does not reach the veins. This leads to the excellent depiction of parenchymal perfusion and the absence of vascular signal on most ASL images. However, if the capillary bed is absent, as in the two most common shunt lesions of the CNS, the arteriovenous malformation and dural arteriovenous fistula, the ASL signal appears in venous structures (69). This can be striking given the high blood volume of the veins (Fig 7).

While large arteriovenous malformations and dural arteriovenous fistulas are not difficult to diagnose with routine anatomic MR imaging, small lesions or evolution of lesions following embolization therapies can be very challenging to identify. Le et al (70) demonstrated that identification of small (< 2 cm) lesions was significantly improved if readers were allowed to view ASL images in addition to conventional images. In fact, this may be more sensitive than conventional angiography, as venous signal on ASL images has been seen in arteriovenous malformations in the setting of intracranial hemorrhage, where initial angiograms were negative, possibly due to the mass effect. It has also been shown that identification of such lesions outside the brain, within the upper neck region, is also possible with ASL (71). Finally, arteriovenous shunting has been identified in about 10% of developmental venous anomalies, suggesting that transitional lesions might be more common than is generally appreciated (72).

One challenge for ASL when venous signal is used to identify shunt lesions is that conspicuity depends on the precise timing parameters (ie, the labeling duration and the postlabel delay). While the use of recommended parameters (10) appears fairly sensitive for detecting most lesions, it is possible that in either slow or fast shunting lesions venous ASL signal could be suboptimal or missed. Therefore, there is interest in multidelay ASL, in which images at different labeling duration and/or postlabel delay are acquired as part of a single acquisition. While these sequences were first developed for better CBF quantification, the ability to optimize the sensitivity for the detection of venous signal is also enhanced. However, spatial resolution is reduced compared with that in single-delay ASL for a given imaging duration, and thus any gains might be offset by this lower resolution. ASL-based multidelay MR angiographic sequences have also been developed, focusing more on direct vessel visualization (73). As such, these latter sequences would compete more directly with conventional angiography, with comparable temporal resolution without the associated risks.

Figure 6

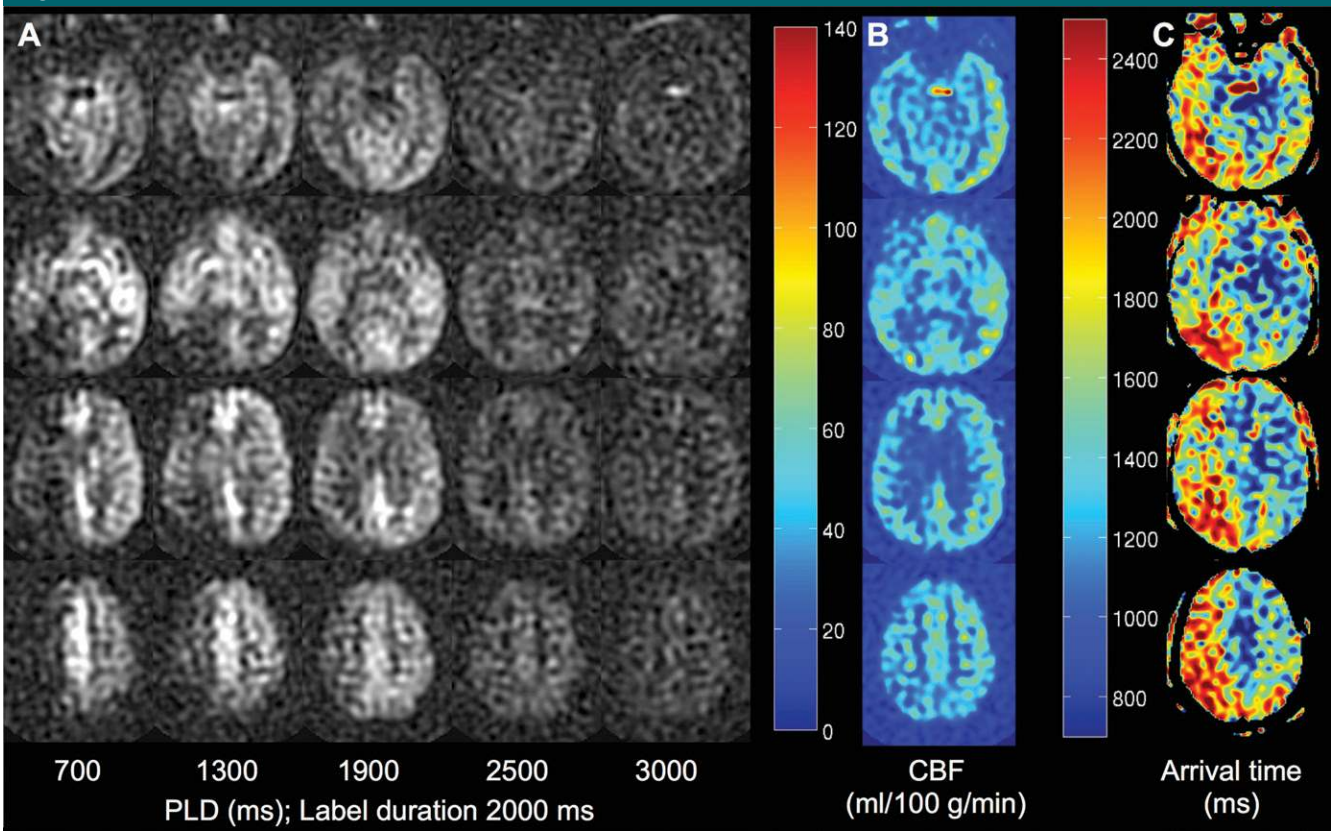

Figure 6: Example of multidelay ASL imaging. A fixed labeling duration of 2000 msec is used, but on subsequent images, different postlabel delays *(PLD)* ranging from 700 to 3000 msec are used, yielding ASL difference (control label) images as shown in *A*. From these data, and the use of general kinetic modeling, one can simultaneously measure, *B,* an arrival-time–corrected CBF and, *C,* the arterial arrival time itself. In this patient, there is near symmetric CBF but clear arterial arrival delay in the right hemisphere, as shown by the higher values on the arrival time map.

ASL in Epilepsy

The main interest of ASL in the context of epilepsy is to locate a potential epileptogenic focus. ASL might further be helpful in the differential diagnosis, for example, in assessing for a stroke in the acute stage. During the acute peri-ictal period, the CBF is typically increased due to pathologic neuronal activity (74), while in the chronic interictal period, CBF is typically reduced as the epileptogenic region typically is less functional and active compared with the normal brain tissue (75–79).

Nuclear medicine techniques such as ictal and interictal single photon emission computed tomography (SPECT) and PET are often performed to detect metabolic changes related to epileptic activity. Since standard structural MR imaging is routinely performed, ASL might be of interest as an additional functional marker of cerebral perfusion with minimal additional effort. Hypoperfusion on ASL images corresponds to hypoperfusion on interictal PET images and electrophysiological data (75,76,80), indicating the potential use of ASL for epileptic focus localization (Fig 8).

ASL in Neoplasms

Hemodynamic changes are present in many central nervous system neoplasms, and in general, CBF and cerebral blood volume (CBV) increase with tumor grade. Historically, much of our MR imaging–based knowledge about these hemodynamic changes has been gained from DSC and dynamic contrast-enhanced imaging (81–87). This has had two main consequences: *(a)* most literature has focused on relative CBV changes, because the DSC measurement of CBV is more straightforward compared with CBF, and *(b)* most of our data are of relatively poor spatial resolution and prone to artifacts, since the rapid passage of the intravascularly confined tracer necessitates rapid, sometimes suboptimal, imaging. ASL cannot measure relative CBV; instead, CBF measurements are more straightforward. While CBV and CBF are related via the Grubb law ($CBV = CBF^{0.38}$) in normal tissue (88), it is likely that this relationship is altered in tumors, which may form abnormal blood vessels that alter the CBV/CBF ratio. Also, since there is no requirement to accurately track a rapid

Figure 7

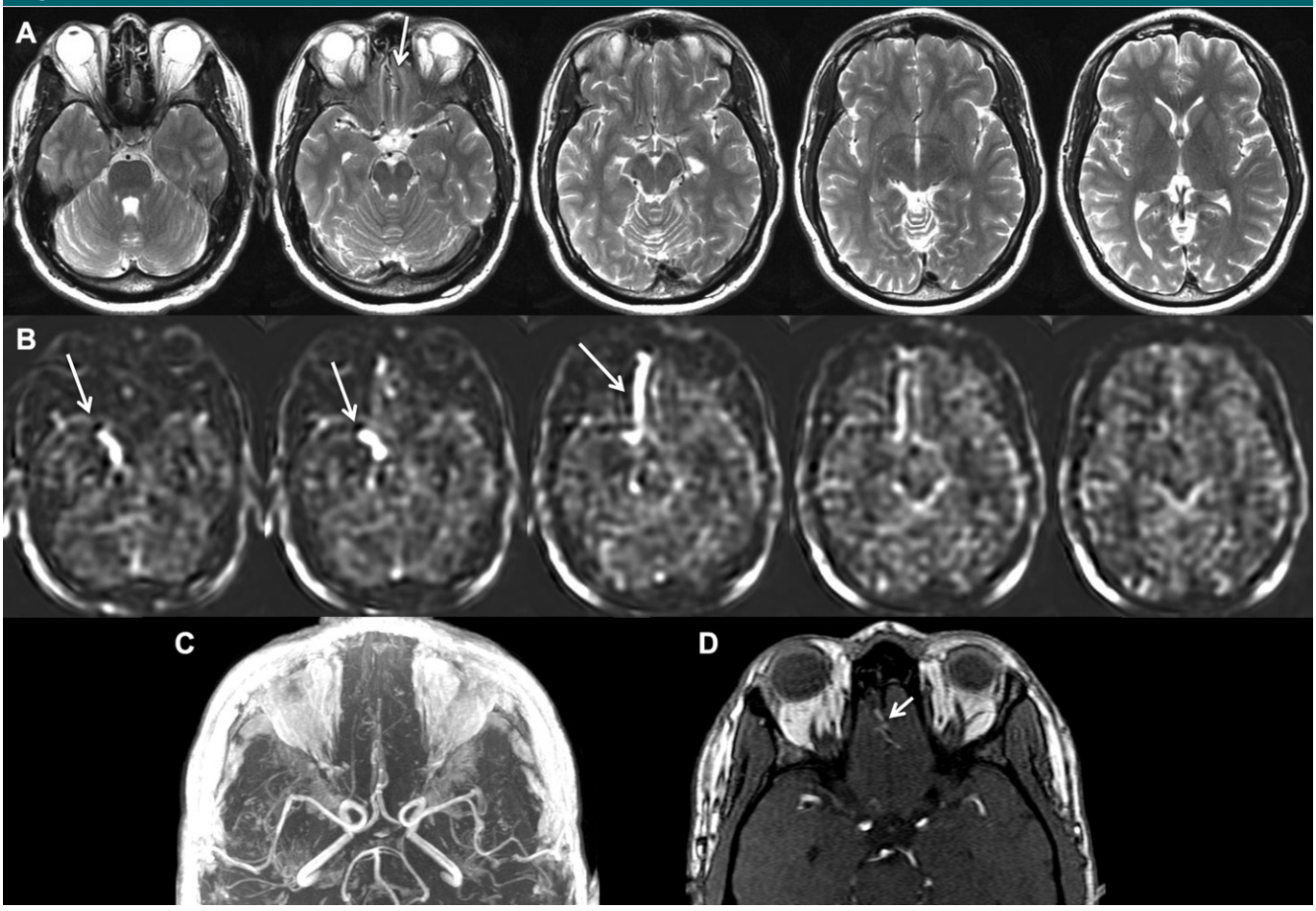

Figure 7: Images in 51-year-old man with exertional headaches and an arteriovenous fistula imaged at 1.5 T. *A,* T2-weighted images demonstrate very subtle flow voids in the inferior frontal lobe (arrow). *B,* ASL images demonstrate linear high signal intensity (arrows) in the region of the right inferior frontal lobe, which extends to the right cavernous sinus, indicative of an arteriovenous shunt lesion. *C,* Collapsed and, *D,* source MR angiographic images confirm the presence of an ethmoid dural fistula (arrow), which was recognized only after the observation of the abnormal ASL signal within the venous structures draining the fistula. This case also demonstrates that while 3 T is preferable to 1.5 T, relevant clinical information can be obtained with ASL at 1.5 T.

intravascular bolus of contrast material, the ASL experiment is more flexible, such that the SNR, spatial resolution, amount of tolerable image distortion, and imaging time may be traded off against one another. Last, since water has high permeability in the normal and neoplastic tissue, there is no need with ASL (unlike DSC) to use complicated leakage-correction algorithms to obtain quantitative results.

Primary Central Nervous System Neoplasms

Glioblastoma multiforme is the most common high-grade central nervous system tumor in adults and is associated with high metabolism and CBF (Fig 9). Initial reports demonstrated that ASL and DSC show largely concordant results in terms of identifying this tumor and distinguishing it from contrast-enhancing mimics (89–92). Higher CBF in glioblastoma multiforme correlates with genetic markers (such as epidermal growth factor receptor) and is associated with shorter progression-free survival time (93). Lower grade tumors typically demonstrate lower CBF. CBF changes may portent transformation to a more aggressive phenotype. In fact, some have suggested that CBF quantification provides a better estimate of event-free survival for a wide range of gliomas than does a histologic grading scale (94). One exception to this rule of increasing CBF and tumor grade is oligodendroglioma, a grade 2 tumor that often demonstrates increased CBF.

Secondary Central Nervous System Lesions

Most metastatic brain lesions show similar or lower glucose uptake and CBF compared with gray matter. However, several metastatic lesions demonstrate increased CBF and share the feature of high vascularity. These include renal cell carcinoma (95), angiosarcoma, hemangioblastoma (96), and melanoma,

Figure 8

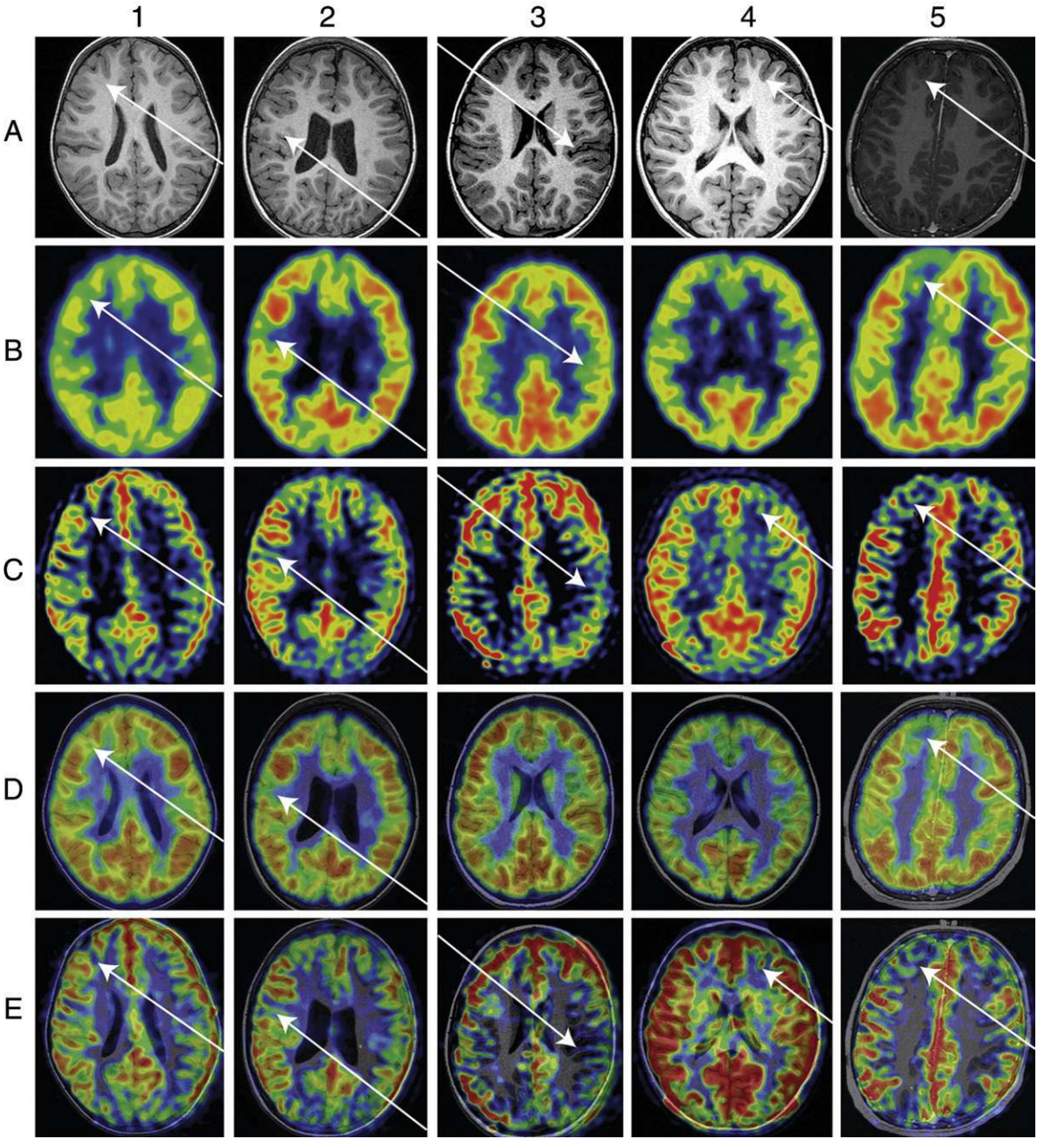

Figure 8: Comparison of ASL MR imaging and FDG PET in epilepsy. Each column represents imaging studies of a single patient. *A,* Preoperative axial T1-weighted MR images. *B,* Raw FDG PET images. *C,* Raw PASL CBF maps. *D,* Image fusion of T1-weighted MR imaging and FDG PET. *E,* Image fusion of T1-weighted MR imaging and PASL. Arrows indicate regions of focal cortical dysplasia that are epileptogenic. Numbers 1–5 refer to different patients. (Reprinted, with permission, from reference 80.)

and in these cases, ASL may be helpful (Fig 10).

Assessing Treatment Response

The quantitative nature of ASL has enabled studies of CBF changes over time or with treatment to assess its impact on prognosis and outcome. A particularly important and challenging distinction to make is between radiation necrosis and recurrent tumor in patients with new or increasing contrast enhancement. Since radiation necrosis is associated typically with reduced CBF and most recurrent tumors demonstrate increased CBF, perfusion imaging may be helpful to distinguish the two entities. DSC and MR spectroscopy

Figure 9

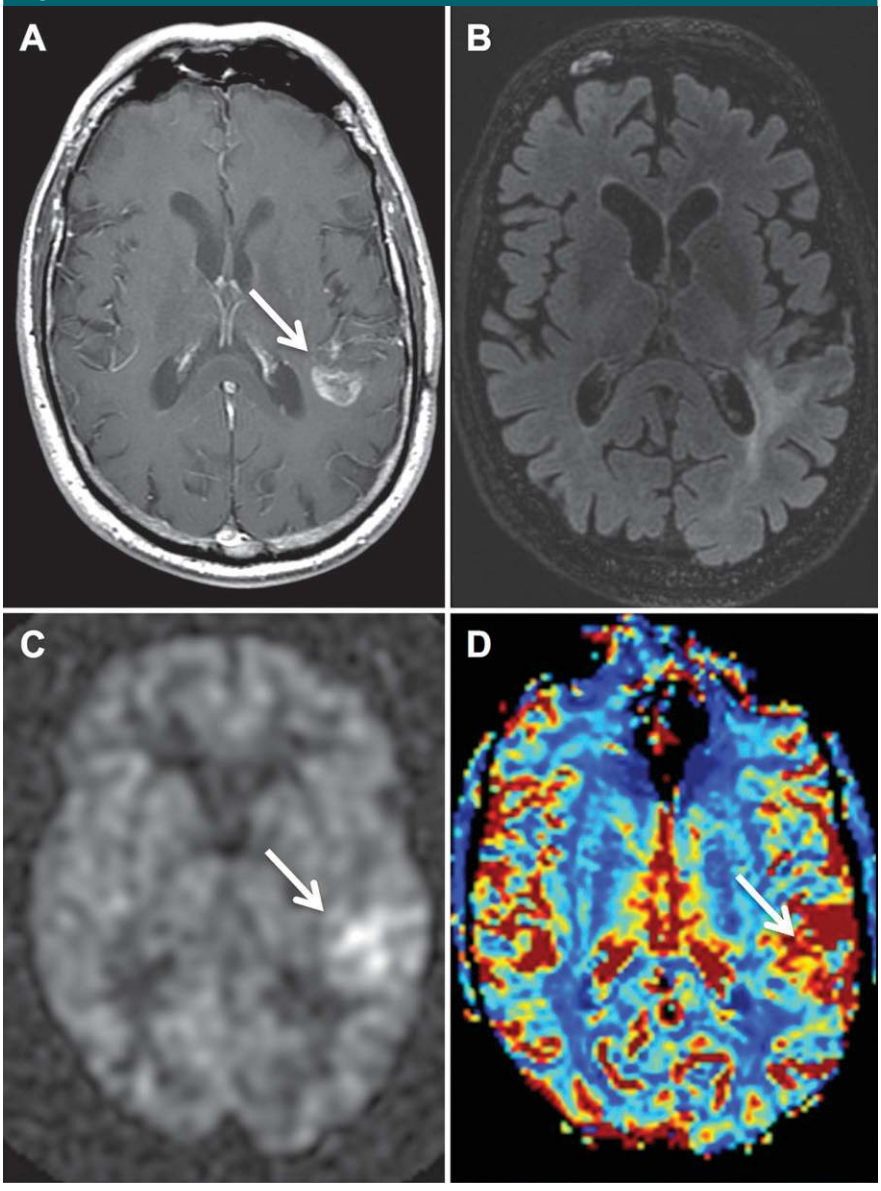

Figure 9: Images in 78-year-old man with unresectable anaplastic astrocytoma (arrow) (World Health Organization Grade 3), seen on, *A,* postcontrast T1-weighted and, *B,* FLAIR images. *C,* ASL image demonstrates increased CBF (arrow) in the region of the tumor. *D,* Increased cerebral blood volume (arrow) is also visible on bolus DSC image, though it is more difficult to appreciate due to the extensive number of arterial and venous vessels that surround the tumor. The findings of high CBF are characteristic of high-grade (grades III and IV) glial neoplasms.

have also been used for this distinction, with some success (97–99). ASL is likely to improve upon DSC perfusion measures, given its better imaging performance around resection cavities (where blood products can affect DSC results). It is also less sensitive to the presence of surrounding large vessels, which can make it challenging to quantify CBF in the actual lesion (Fig 11).

Using clinical and imaging end points, Oszunar et al (100) suggested that ASL is superior to FDG PET and DSC for distinguishing tumor recurrence from radiation necrosis in gliomas, with a sensitivity of 94%. In the early time period following resection (< 4 weeks), where any contrast enhancement is probably due to pseudoprogression, again ASL appeared more useful than DSC (101). Another technique that can evaluate both initial presentation and treatment changes in tumors is dynamic contrast-enhanced imaging, in which the rate of contrast agent leakage is estimated.

ASL in Psychiatric and Other Neurologic Disorders

An increasing number of investigations have assessed ASL in various psychiatric and neurologic diseases.

Depression

In a study of 25 medication-naive adolescents with major depressive disorder, Ho et al found a complex pattern of hypoperfusion in frontal, limbic, paralimbic, and cingulate yet hyperperfusion within the subcallosal cingulate, putamen, and fusiform gyrus (102). The authors conclude that adolescents with major depressive disorder differ in their baseline perfusion in executive, affective, and motor networks. Several studies assessed adults with depression and found reduced CBF in the default mode network (103) (a brain network initially described on the basis of CBF maps [104] that is consistently found in resting-state functional MR imaging studies [105]), as well as bilateral subgenual anterior cingulate cortex, left prefrontal dorso-median cortex, and left subcortical areas (putamen, pallidum and amygdala) (106). Lui et al further subdivided patients with refractory depressive disorder from patients with nonrefractory depressive disorder (107). Subjects with nonrefractory depressive disorder versus control subjects had reduced CBF in the left prefrontal cortex and increased CBF mainly in the limbic-striatal areas. Conversely, subjects with refractory depressive disorder had decreased CBF predominantly in the bilateral frontal and bilateral thalamic regions. The direct comparison of the two depressive disorder groups further

Figure 10

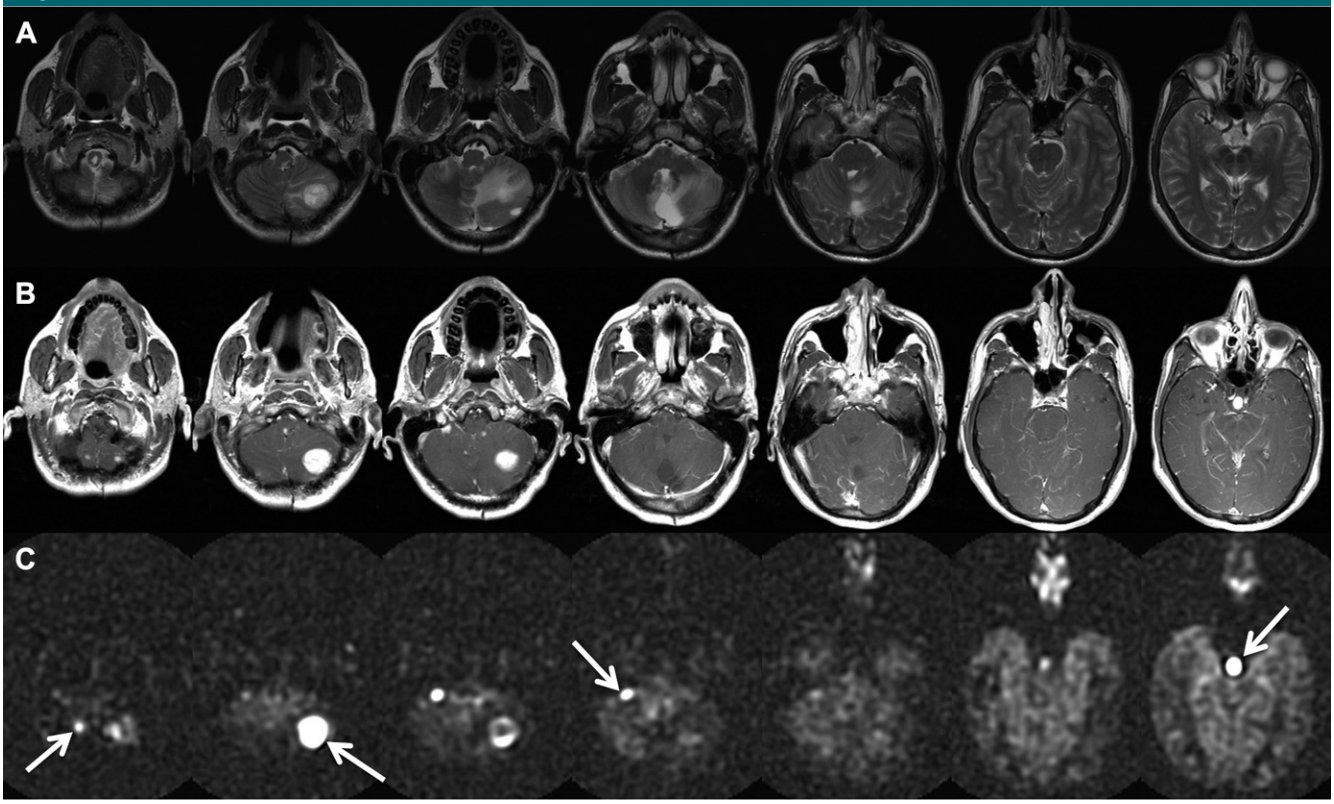

Figure 10: *A,* T2-weighted, *B,* postcontrast T1-weighted, and *C,* ASL images in a 40-year-old man with von Hippel Lindau disease and multiple hemangioblastomas after multiple prior surgeries. Arrows point to the extremely high CBF measured with ASL even in very small lesions.

revealed higher CBF mainly in the limbic-striatal areas. Finally, late-life depression is associated with increased white matter CBF yet conserved gray matter CBF (108). In conclusion, these results indicate that different subtypes of depression are associated with specific patterns of CBF alterations, which furthermore change over the lifespan.

Psychosis

Patients with schizophrenia compared with control subjects had a pattern of increased CBF in left putamen/superior corona radiata and right middle temporal gyrus yet decreased CBF in bilateral precuneus and middle frontal gyrus (109). Moreover, a subdivision of patients according to symptoms revealed an association of negative symptoms (including difficulties in thinking or coming up with ideas, decreased ability to initiate tasks, lowered levels of motivation or drive, lack of interest in other people) with reduced CBF in bilateral superior temporal gyrus, cingulate gyrus, and left middle frontal gyrus and an association of positive symptoms (including delusions, hallucinations, disorganized speech or behavior) with increased CBF in cingulate gyrus and superior frontal gyrus and decreased CBF in precentral gyrus/middle frontal gyrus. A study by Ota et al (110) found a different pattern of reduced relative CBF in the left prefrontal and bilateral occipital cortices compared with the healthy volunteers. Finally, Kindler et al (111) observed decreased mean CBF in the frontal and temporal regions and significantly increased default mode network connectivity in the precuneus in patients with schizophrenia. Currently it is impossible to disentangle whether these observed differences in ASL-based alterations in CBF in schizophrenia patients are due to different stages and subtypes of the disease, are methodological, or a combination of both.

Posttraumatic Stress Disorder

Posttraumatic stress disorder (PTSD) has attracted considerable interest in recent years. Schuff et al (112) assessed 17 male veterans with PTSD and observed increased relative CBF in primarily right parietal and superior temporal cortices. Li et al (113) implemented a more complex setup in veterans nearly 20 years after the 1991 Gulf War, contrasting baseline ASL with a physostigmine challenge. Physostigmine significantly decreased hippocampal relative CBF in control subjects and veterans with syndrome 1 (impaired cognition), yet significantly increased hippocampal relative CBF in veterans with syndrome 2 (confusion-ataxia) and 3 (central neuropathic pain), suggesting that ASL might differentiate subtypes of PTSD types.

Figure 11

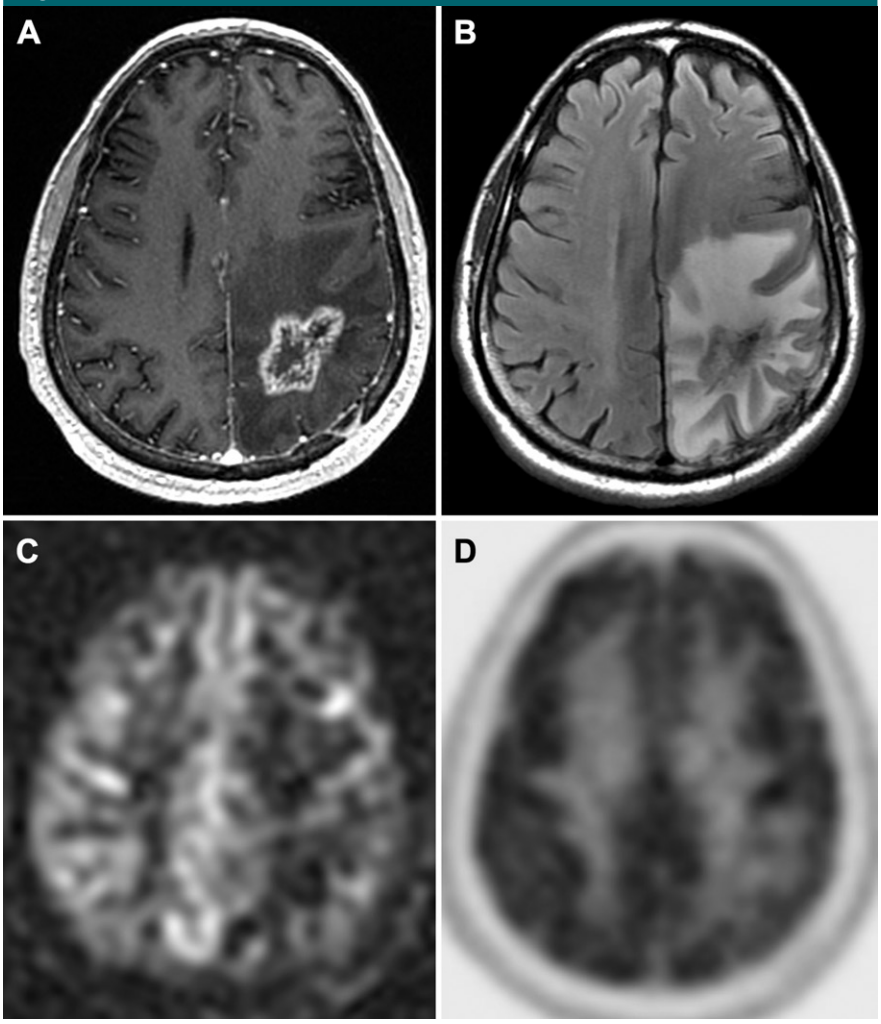

Figure 11: Images in 57-year-old man with lung cancer brain metastasis 15 months after resection, radiation, and chemotherapy. *A,* Axial T1-weighted gadolinium-enhanced image shows a new enhancing lesion, with, *B,* axial fluid-attenuated inversion recovery image demonstrating extensive vasogenic edema in the region of the resection cavity. C, ASL image demonstrates no increase in CBF in this region, similar to findings on, *D,* FDG PET image. These findings were considered to represent radiation necrosis and the patient is being followed serially rather than with re-resection.

Mild Traumatic Brain Injury

Mild traumatic brain injury (MTBI) is another entity that has attracted considerable interest, notably related to the discussion of brain alterations in professional football and soccer players. Conventional MR imaging sequences are not sensitive enough to detect structural brain changes, and consequently an increasing number of investigations used advanced imaging techniques such as ASL or diffusion-weighted imaging (114). In 2009, Ge et al (115) demonstrated reduced CBF in bilateral thalamus in patients with MTBI. Later on, the same group extended these findings in the assessment of CBF by combining ASL and diffusion-tensor and diffusion kurtosis imaging to assess the white matter, again detecting substantial alterations in both perfusion and white matter integrity in MTBI patients, focusing on the thalamus (114). Interestingly these alterations persisted more than 9 months after injury. Doshi et al (116) assessed the acute stage of MTBI and found increased regional CBF in the left striatum and in frontal and occipital lobes. Finally, Wang et al (117) investigated MTBI in pediatric patients and found reduced CBF in bilateral frontotemporal regions. In summary, these results indicate that ASL might be a sensitive marker to assess MTBI-related alterations in the brain, which are not detectable with conventional MR imaging techniques. The discrepancies between these studies in turn also imply the need for strict standardization of both data acquisition and data analysis.

Pain and Migraine

Owen et al (118) investigated healthy volunteers during painful thermal stimulation and observed bilateral CBF changes that included the insula, secondary somatosensory, and cingulate cortices, as well as the supplementary motor area, in an attempt to quantify pain-induced perfusion alterations in the brain. A similar approach by Maleki et al (119) found alterations in relative CBF in somatosensory cortex, anterior cingulate cortex, anterior insula, hippocampus, amygdala, thalamus, and precuneus. Taken together, these studies suggest that ASL might be used as an operator-independent marker in subjective pain syndromes. Accordingly, Liu et al observed, in patients with postherpetic neuralgia, a pattern of increased CBF in left striatum, right thalamus, left primary somatosensory cortex, left insula, left amygdala, left primary somatomotor cortex, and left inferior parietal lobule yet decreases CBF in the frontal cortex (120).

Migraine is of particular interest with respect to ASL imaging. Although controversial, it is thought that migraine attacks might involve vascular dysregulation. Correspondingly, mapping the brain CBF by means of ASL might reveal insights into the pathophysiology of migraine. Kato et al performed ASL imaging in a patient during a migraine attack, after treatment with a triptan and in the attack-free period (121). During the migraine attack, the CBF was reduced in bilateral median thalamic areas, including hypothalamus,

Figure 12

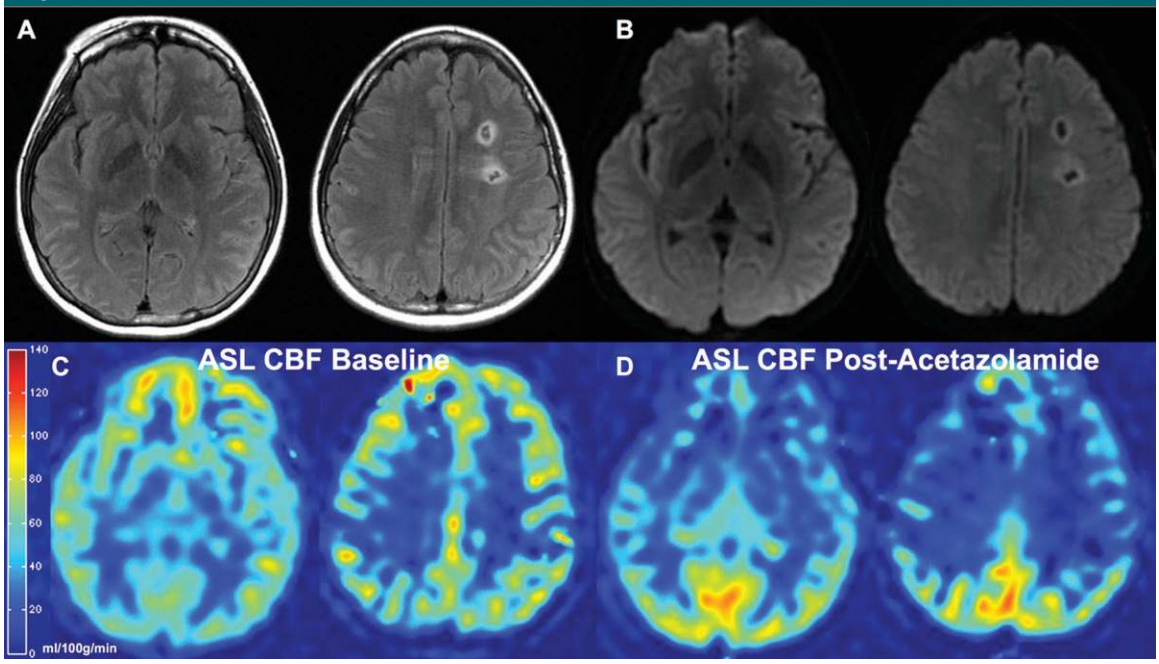

Figure 12: Images in 29-year-old woman with bilateral Moyamoya disease. Both, *A,* fluid-attenuated inversion recovery and, *B,* diffusion-weighted images show evidence of prior infarcts in the deep white matter on the left side. *C,* Multidelay ASL image acquired at baseline shows normal CBF in the bilateral anterior circulation. *D,* However, image obtained 10 minutes after intravenous administration of 1 g of acetazolamide demonstrates the expected CBF increase in the posterior circulation but marked reduction in CBF in both anterior circulations, compatible with cerebrovascular steal. This finding has been associated with a high risk of subsequent cerebrovascular events and prompted bilateral direct superficial temporal artery-middle cerebral artery bypass.

and increased in the frontal cortex as compared with baseline. Thirty minutes after treatment initiation, CBF perfusion improved in the thalamus and hypothalamus. A case series by Pollock et al demonstrated regional cerebral hyperperfusion in three of 11 patients during a headache episode that corresponded to previous aura symptoms (122). While these pilot studies demonstrated interesting preliminary findings, larger scale studies are clearly needed to investigate whether ASL might contribute to a better understanding of the pathophysiology of pain, notably a potential vascular component of migraine.

Extensions of ASL

Superselective ASL to Map Vascular Territories (Also Known as Selective Territory Mapping)

Contrary to contrast-enhanced CT perfusion or DSC, ASL provides the opportunity to selectively label vascular territories, such as left carotid, right carotid, and vertebrobasilar territories (123,124) or even their more distal branches. This can be of interest from a scientific perspective, for example, to assess the impact of vascular variants of the circle of Willis on perfusion of the brain tissue, such as caudate and lenticular nucleus and thalamus (125). More important, territorial ASL might have clinical value, for example, to determine whether multiple acute vascular lesions are in the same vascular territory as argument for distant cardioembolic events in several vascular territories versus local stenotic origin for a single vascular territory or for neurosurgical planning of, for example, aneurysm clipping or tumor resection.

Cerebrovascular Reserve Imaging

The ability of an organ to adapt to a physiologic challenge, particularly one that stresses its limits, can be measured by using reserve studies. Such imaging may unmask deficits that are not apparent on routine images. Myocardial stress-rest imaging following either exercise or pharmaceutical vasodilatory challenge has been a mainstay of cardiac imaging for decades. A similar cerebrovascular "stress test" can be performed by using either physiologic (ie, CO_2 inhalation or breath hold) or pharmaceutical vasodilation. In particular, acetazolamide, a carbonic anhydrase inhibitor, causes 20%–50% CBF increase in healthy subjects. However, patients in whom the cerebrovasculature is already maximally dilated to maintain baseline CBF may not be able to augment their CBF further in response to an acetazolamide challenge. In fact, those with very severe disease may demonstrate reduced CBF in response to challenge, a phenomenon known as cerebrovascular steal.

Limited data on use of non–MR imaging techniques, including transcranial

Figure 13

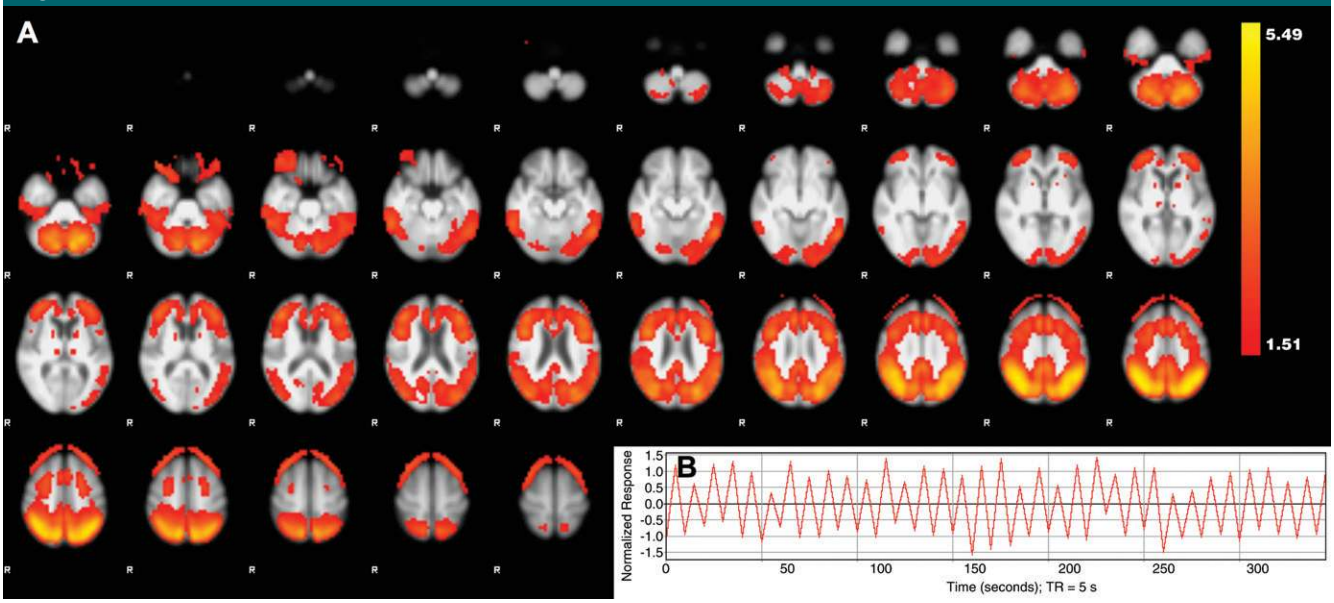

Figure 13: Functional connectivity analysis of ASL raw data in 154 healthy elderly control subjects and 66 cases with mild cognitive impairment. Note that for illustrative purposes, the raw ASL data were directly analyzed by using tensorial independent component in FSL *(www.fmrib.ox.ac.uk/fsl/)*, an established technique optimized for functional MR imaging analysis. *A,* Spatial representation of one of the independent components. *B,* The on-off labeling pattern of the raw ASL data is clearly visible on the corresponding temporal representation. Currently ongoing methodological adaptation and optimization to the specific properties of ASL data, such as implementing the known prior knowledge of the on-off time course, will improve the quality of ASL-derived functional connectivity networks.

Doppler, SPECT, and PET, suggest that demonstration of poor reserve is an important risk factor for subsequent cerebrovascular events (126). Given its noninvasive nature, ASL is an ideal method to image CBF changes in response to a challenge (14,127). Since these patients may have large artery stenosis or occlusion, the use of multidelay ASL to quantify both arrival time and CBF is recommended. An example of reserve imaging with multidelay ASL in a patient with Moyamoya disease with cerebrovascular steal of the bilateral anterior circulation is shown in Figure 12.

Functional MR Imaging and ASL

Functional MR imaging studies generally rely on the blood oxygen level–dependent (BOLD) effect (128) and neurovascular coupling (129). Because functional MR imaging does not directly measure neuronal activation but the indirect vascular response, alterations of the neurovascular coupling might influence the resulting functional MR imaging BOLD signal, for example, already in normal aging (33,130). The combination of ASL and functional MR imaging might disentangle vascular and neuronal contributions of the BOLD response (130). Moreover, it is possible to use the time series of the ASL raw data to calculate functional MR imaging activation maps (131) or resting-state functional connectivity networks known from functional MR imaging (105). Although the quality of these ASL-based results is generally below that of classic echo-planar BOLD functional MR imaging, this might be interesting from a clinical perspective as ASL can be used to calculate relative CBF maps and resting-state functional connectivity networks of a reasonable quality without additional cost or imaging time, which is particularly helpful in elderly patients (Fig 13).

Conclusion

Although ASL has been around for more than 2 decades, it only recently began to make the transition from a research tool to clinical use due to increasing awareness of radiologists and clinicians of its capability and technical improvements that have made this approach more reliable and available as product sequences on MR imaging platforms. For many diseases, including dementia, vascular diseases, neoplasms, and various psychiatric diseases, ASL provides additional and complementary information to that available from structural MR imaging. Current methodological developments aim to increase the robustness and decrease interimager variability of CBF estimation.

Disclosures of Conflicts of Interest: S.H. disclosed no relevant relationships. **G.Z.** Activities related to the present article: institution received a grant from NIH. Activities not related to the present article: institution received grants from GE Healthcare for research support. Other relationships: disclosed no relevant relationships. **D.L.T.** disclosed no relevant relationships. **K.O.L.** disclosed no relevant relationships. **F.B.** Activities related to the present article: disclosed no relevant relationships. Activities not related to the present article: author received consultancy fees from Bayer-Schering, Sanofi-Aventis, and Genzyme; author and institution received consultancy fees from Biogen-Idec, TEVA, Merck-Serono, Novartis, Roche, Synthon BV, Jansen Research; institution received grants from Dutch MS Society, EU-FP7 and author received hono-

raria; author received payment for development of educational presentations including service on speakers' bureaus from Serono Symposia Foundation and MedScape. Other relationships: disclosed no relevant relationships. **X.G.** Activities related to the present article: disclosed no relevant relationships. Activities not related to the present article: CEO, Gold Standard Phantoms. Other relationships: disclosed no relevant relationships.

References

1. Detre JA, Leigh JS, Williams DS, Koretsky AP. Perfusion imaging. Magn Reson Med 1992;23(1):37–45.
2. Williams DS, Detre JA, Leigh JS, Koretsky AP. Magnetic resonance imaging of perfusion using spin inversion of arterial water. Proc Natl Acad Sci U S A 1992;89(1):212–216.
3. Roberts DA, Detre JA, Bolinger L, Insko EK, Leigh JS Jr. Quantitative magnetic resonance imaging of human brain perfusion at 1.5 T using steady-state inversion of arterial water. Proc Natl Acad Sci U S A 1994;91(1):33–37.
4. Golay X, Petersen ET. Arterial spin labeling: benefits and pitfalls of high magnetic field. Neuroimaging Clin N Am 2006;16(2):259–268, x.
5. Kety SS, Schmidt CF. The nitrous oxide method for the quantitative determination of cerebral blood flow in man: theory, procedure and normal values. J Clin Invest 1948;27(4):476–483.
6. Kety SS, Schmidt CF. The determination of cerebral blood flow in man by use of nitrous oxide in low concentrations. Am J Physiol 1945;143(1):53–66.
7. Vidorreta M, Wang Z, Rodríguez I, Pastor MA, Detre JA, Fernández-Seara MA. Comparison of 2D and 3D single-shot ASL perfusion fMRI sequences. Neuroimage 2013;66:662–671.
8. Vidorreta M, Balteau E, Wang Z, et al. Evaluation of segmented 3D acquisition schemes for whole-brain high-resolution arterial spin labeling at 3 T. NMR Biomed 2014;27(11):1387–1396.
9. Dai W, Garcia D, de Bazelaire C, Alsop DC. Continuous flow-driven inversion for arterial spin labeling using pulsed radio frequency and gradient fields. Magn Reson Med 2008;60(6):1488–1497.
10. Alsop DC, Detre JA, Golay X, et al. Recommended implementation of arterial spin-labeled perfusion MRI for clinical applications: a consensus of the ISMRM perfusion study group and the European consortium for ASL in dementia. Magn Reson Med 2015;73(1):102–116.
11. Alsop DC, Detre JA. Reduced transit-time sensitivity in noninvasive magnetic resonance imaging of human cerebral blood flow. J Cereb Blood Flow Metab 1996;16(6):1236–1249.
12. Wong EC, Buxton RB, Frank LR. Quantitative imaging of perfusion using a single subtraction (QUIPSS and QUIPSS II). Magn Reson Med 1998;39(5):702–708.
13. Deibler AR, Pollock JM, Kraft RA, Tan H, Burdette JH, Maldjian JA. Arterial spin-labeling in routine clinical practice. II. Hypoperfusion patterns. AJNR Am J Neuroradiol 2008;29(7):1235–1241.
14. Detre JA, Samuels OB, Alsop DC, Gonzalez-At JB, Kasner SE, Raps EC. Noninvasive magnetic resonance imaging evaluation of cerebral blood flow with acetazolamide challenge in patients with cerebrovascular stenosis. J Magn Reson Imaging 1999;10(5):870–875.
15. Zaharchuk G, Bammer R, Straka M, et al. Arterial spin-label imaging in patients with normal bolus perfusion-weighted MR imaging findings: pilot identification of the borderzone sign. Radiology 2009;252(3):797–807.
16. Bokkers RP, Bremmer JP, van Berckel BN, et al. Arterial spin labeling perfusion MRI at multiple delay times: a correlative study with H(2)(15)O positron emission tomography in patients with symptomatic carotid artery occlusion. J Cereb Blood Flow Metab 2010;30(1):222–229.
17. Petersen ET, Lim T, Golay X. Model-free arterial spin labeling quantification approach for perfusion MRI. Magn Reson Med 2006;55(2):219–232.
18. Jack CR Jr, Knopman DS, Jagust WJ, et al. Hypothetical model of dynamic biomarkers of the Alzheimer's pathological cascade. Lancet Neurol 2010;9(1):119–128.
19. Brown RK, Bohnen NI, Wong KK, Minoshima S, Frey KA. Brain PET in suspected dementia: patterns of altered FDG metabolism. RadioGraphics 2014;34(3):684–701.
20. Buxton RB, Frank LR. A model for the coupling between cerebral blood flow and oxygen metabolism during neural stimulation. J Cereb Blood Flow Metab 1997;17(1):64–72.
21. Aubert A, Costalat R. A model of the coupling between brain electrical activity, metabolism, and hemodynamics: application to the interpretation of functional neuroimaging. Neuroimage 2002;17(3):1162–1181.
22. Yoshiura T, Hiwatashi A, Noguchi T, et al. Arterial spin labelling at 3-T MR imaging for detection of individuals with Alzheimer's disease. Eur Radiol 2009;19(12):2819–2825.
23. Yoshiura T, Hiwatashi A, Yamashita K, et al. Simultaneous measurement of arterial transit time, arterial blood volume, and cerebral blood flow using arterial spin-labeling in patients with Alzheimer disease. AJNR Am J Neuroradiol 2009;30(7):1388–1393.
24. Dai W, Lopez OL, Carmichael OT, Becker JT, Kuller LH, Gach HM. Mild cognitive impairment and alzheimer disease: patterns of altered cerebral blood flow at MR imaging. Radiology 2009;250(3):856–866.
25. Binnewijzend MA, Kuijer JP, Benedictus MR, et al. Cerebral blood flow measured with 3D pseudocontinuous arterial spin-labeling MR imaging in Alzheimer disease and mild cognitive impairment: a marker for disease severity. Radiology 2013;267(1):221–230.
26. Wolk DA, Detre JA. Arterial spin labeling MRI: an emerging biomarker for Alzheimer's disease and other neurodegenerative conditions. Curr Opin Neurol 2012;25(4):421–428.
27. Bozoki AC, Korolev IO, Davis NC, Hoisington LA, Berger KL. Disruption of limbic white matter pathways in mild cognitive impairment and Alzheimer's disease: a DTI/FDG-PET study. Hum Brain Mapp 2012;33(8):1792–1802.
28. Pagani M, Dessi B, Morbelli S, et al. MCI patients declining and not-declining at midterm follow-up: FDG-PET findings. Curr Alzheimer Res 2010;7(4):287–294.
29. Herholz K, Salmon E, Perani D, et al. Discrimination between Alzheimer dementia and controls by automated analysis of multicenter FDG PET. Neuroimage 2002;17(1):302–316.
30. Du AT, Jahng GH, Hayasaka S, et al. Hypoperfusion in frontotemporal dementia and Alzheimer disease by arterial spin labeling MRI. Neurology 2006;67(7):1215–1220.
31. Biagi L, Abbruzzese A, Bianchi MC, Alsop DC, Del Guerra A, Tosetti M. Age dependence of cerebral perfusion assessed by magnetic resonance continuous arterial spin labeling. J Magn Reson Imaging 2007;25(4):696–702.
32. Lee C, Lopez OL, Becker JT, et al. Imaging cerebral blood flow in the cognitively normal aging brain with arterial spin labeling: implications for imaging of neurodegenerative disease. J Neuroimaging 2009;19(4):344–352.
33. Restom K, Bangen KJ, Bondi MW, Perthen JE, Liu TT. Cerebral blood flow and BOLD

responses to a memory encoding task: a comparison between healthy young and elderly adults. Neuroimage 2007;37(2):430–439.

34. Rusinek H, Brys M, Glodzik L, et al. Hippocampal blood flow in normal aging measured with arterial spin labeling at 3T. Magn Reson Med 2011;65(1):128–137.

35. Xekardaki A, Rodriguez C, Montandon ML, et al. Arterial spin labeling may contribute to the prediction of cognitive deterioration in healthy elderly individuals. Radiology 2015;274(2):490–499.

36. Jack CR Jr, Knopman DS, Jagust WJ, et al. Tracking pathophysiological processes in Alzheimer's disease: an updated hypothetical model of dynamic biomarkers. Lancet Neurol 2013;12(2):207–216.

37. Alsop DC, Detre JA, Grossman M. Assessment of cerebral blood flow in Alzheimer's disease by spin-labeled magnetic resonance imaging. Ann Neurol 2000;47(1):93–100.

38. Musiek ES, Chen Y, Korczykowski M, et al. Direct comparison of fluorodeoxyglucose positron emission tomography and arterial spin labeling magnetic resonance imaging in Alzheimer's disease. Alzheimers Dement 2012;8(1):51–59.

39. Chen Y, Wolk DA, Reddin JS, et al. Voxel-level comparison of arterial spin-labeled perfusion MRI and FDG-PET in Alzheimer disease. Neurology 2011;77(22):1977–1985.

40. Chao LL, Buckley ST, Kornak J, et al. ASL perfusion MRI predicts cognitive decline and conversion from MCI to dementia. Alzheimer Dis Assoc Disord 2010;24(1):19–27.

41. Verfaillie SC, Adriaanse SM, Binnewijzend MA, et al. Cerebral perfusion and glucose metabolism in Alzheimer's disease and frontotemporal dementia: two sides of the same coin? Eur Radiol 2015;25(10):3050–3059.

42. Taylor JP, Firbank MJ, He J, et al. Visual cortex in dementia with Lewy bodies: magnetic resonance imaging study. Br J Psychiatry 2012;200(6):491–498.

43. Le Heron CJ, Wright SL, Melzer TR, et al. Comparing cerebral perfusion in Alzheimer's disease and Parkinson's disease dementia: an ASL-MRI study. J Cereb Blood Flow Metab 2014;34(6):964–970.

44. Schuff N, Matsumoto S, Kmiecik J, et al. Cerebral blood flow in ischemic vascular dementia and Alzheimer's disease, measured by arterial spin-labeling magnetic resonance imaging. Alzheimers Dement 2009;5(6):454–462.

45. Gao YZ, Zhang JJ, Liu H, Wu GY, Xiong L, Shu M. Regional cerebral blood flow and cerebrovascular reactivity in Alzheimer's disease and vascular dementia assessed by arterial spinlabeling magnetic resonance imaging. Curr Neurovasc Res 2013;10(1):49–53.

46. Bastos-Leite AJ, Kuijer JP, Rombouts SA, et al. Cerebral blood flow by using pulsed arterial spin-labeling in elderly subjects with white matter hyperintensities. AJNR Am J Neuroradiol 2008;29(7):1296–1301.

47. Firbank MJ, He J, Blamire AM, et al. Cerebral blood flow by arterial spin labeling in poststroke dementia. Neurology 2011;76(17):1478–1484.

48. van Gelderen P, de Zwart JA, Duyn JH. Pitfalls of MRI measurement of white matter perfusion based on arterial spin labeling. Magn Reson Med 2008;59(4):788–795.

49. van Osch MJ, Teeuwisse WM, van Walderveen MA, Hendrikse J, Kies DA, van Buchem MA. Can arterial spin labeling detect white matter perfusion signal? Magn Reson Med 2009;62(1):165–173.

50. Wu WC, Lin SC, Wang DJ, Chen KL, Li YD. Measurement of cerebral white matter perfusion using pseudocontinuous arterial spin labeling 3T magnetic resonance imaging: an experimental and theoretical investigation of feasibility. PLoS One 2013;8(12):e82679.

51. The National Institute of Neurological Disorders and Stroke rt-PA Stroke Study Group. Tissue plasminogen activator for acute ischemic stroke. N Engl J Med 1995;333(24):1581–1587.

52. Siewert B, Schlaug G, Edelman RR, Warach S. Comparison of EPISTAR and T2*-weighted gadolinium-enhanced perfusion imaging in patients with acute cerebral ischemia. Neurology 1997;48(3):673–679.

53. Viallon M, Altrichter S, Pereira VM, et al. Combined use of pulsed arterial spin-labeling and susceptibility-weighted imaging in stroke at 3T. Eur Neurol 2010;64(5):286–296.

54. Zaharchuk G, El Mogy IS, Fischbein NJ, Albers GW. Comparison of arterial spin labeling and bolus perfusion-weighted imaging for detecting mismatch in acute stroke. Stroke 2012;43(7):1843–1848.

55. Bokkers RP, Hernandez DA, Merino JG, et al. Whole-brain arterial spin labeling perfusion MRI in patients with acute stroke. Stroke 2012;43(5):1290–1294.

56. Hernandez DA, Bokkers RP, Mirasol RV, et al. Pseudocontinuous arterial spin labeling quantifies relative cerebral blood flow in acute stroke. Stroke 2012;43(3):753–758.

57. Chng SM, Petersen ET, Zimine I, Sitoh YY, Lim CC, Golay X. Territorial arterial spin labeling in the assessment of collateral circulation: comparison with digital subtraction angiography. Stroke 2008;39(12):3248–3254.

58. Zaharchuk G, Do HM, Marks MP, Rosenberg J, Moseley ME, Steinberg GK. Arterial spin-labeling MRI can identify the presence and intensity of collateral perfusion in patients with moyamoya disease. Stroke 2011;42(9):2485–2491.

59. Altrichter S, Kulcsar Z, Jägersberg M, et al. Arterial spin labeling shows cortical collateral flow in the endovascular treatment of vasospasm after post-traumatic subarachnoid hemorrhage. J Neuroradiol 2009;36(3):158–161.

60. Bivard A, Krishnamurthy V, Stanwell P, et al. Arterial spin labeling versus bolus-tracking perfusion in hyperacute stroke. Stroke 2014;45(1):127–133.

61. Teeuwisse WM, Schmid S, Ghariq E, Veer IM, van Osch MJ. Time-encoded pseudocontinuous arterial spin labeling: basic properties and timing strategies for human applications. Magn Reson Med 2014;72(6):1712–1722.

62. Dai W, Shankaranarayanan A, Alsop DC. Volumetric measurement of perfusion and arterial transit delay using hadamard encoded continuous arterial spin labeling. Magn Reson Med 2013;69(4):1014–1022.

63. Hendrikse J, van Osch MJ, Rutgers DR, et al. Internal carotid artery occlusion assessed at pulsed arterial spin-labeling perfusion MR imaging at multiple delay times. Radiology 2004;233(3):899–904.

64. Bokkers RP, van der Worp HB, Mali WP, Hendrikse J. Noninvasive MR imaging of cerebral perfusion in patients with a carotid artery stenosis. Neurology 2009;73(11):869–875.

65. Noguchi T, Kawashima M, Irie H, et al. Arterial spin-labeling MR imaging in moyamoya disease compared with SPECT imaging. Eur J Radiol 2011;80(3):e557–e562.

66. Saida T, Masumoto T, Nakai Y, Shiigai M, Matsumura A, Minami M. Moyamoya disease: evaluation of postoperative revascularization using multiphase selective arterial spin labeling MRI. J Comput Assist Tomogr 2012;36(1):143–149.

67. Sugino T, Mikami T, Miyata K, Suzuki K, Houkin K, Mikuni N. Arterial spin-labeling magnetic resonance imaging after revascu-

larization of moyamoya disease. J Stroke Cerebrovasc Dis 2013;22(6):811–816.

68. Goetti R, O'Gorman R, Khan N, Kellenberger CJ, Scheer I. Arterial spin labelling MRI for assessment of cerebral perfusion in children with moyamoya disease: comparison with dynamic susceptibility contrast MRI. Neuroradiology 2013;55(5):639–647.
69. Wolf RL, Wang J, Detre JA, Zager EL, Hurst RW. Arteriovenous shunt visualization in arteriovenous malformations with arterial spin-labeling MR imaging. AJNR Am J Neuroradiol 2008;29(4):681–687.
70. Le TT, Fischbein NJ, André JB, Wijman C, Rosenberg J, Zaharchuk G. Identification of venous signal on arterial spin labeling improves diagnosis of dural arteriovenous fistulas and small arteriovenous malformations. AJNR Am J Neuroradiol 2012;33(1):61–68.
71. Alexander M, McTaggart R, Santarelli J, et al. Multimodality evaluation of dural arteriovenous fistula with CT angiography, MR with arterial spin labeling, and digital subtraction angiography: case report. J Neuroimaging 2014;24(5):520–523.
72. Iv M, Fischbein NJ, Zaharchuk G. Association of developmental venous anomalies with perfusion abnormalities on arterial spin labeling and bolus perfusion-weighted imaging. J Neuroimaging 2015;25(2):243–250.
73. Kopeinigg D, Bammer R. Time-resolved angiography using inflow subtraction (TRAILS). Magn Reson Med 2014;72(3):669–678.
74. Nguyen D, Kapina V, Seeck M, Viallon M, Fedespiel A, Lovblad KO. Ictal hyperperfusion demonstrated by arterial spin-labeling MRI in status epilepticus. J Neuroradiol 2010;37(4):250–251.
75. Pendse N, Wissmeyer M, Altrichter S, et al. Interictal arterial spin-labeling MRI perfusion in intractable epilepsy. J Neuroradiol 2010;37(1):60–63.
76. Lim YM, Cho YW, Shamim S, et al. Usefulness of pulsed arterial spin labeling MR imaging in mesial temporal lobe epilepsy. Epilepsy Res 2008;82(2-3):183–189.
77. Storti SF, Boscolo Galazzo I, Del Felice A, et al. Combining ESI, ASL and PET for quantitative assessment of drug-resistant focal epilepsy. Neuroimage 2014;102(Pt 1):49–59.
78. Miyaji Y, Yokoyama M, Kawabata Y, et al. Arterial spin-labeling magnetic resonance imaging for diagnosis of late seizure after stroke. J Neurol Sci 2014;339(1-2):87–90.
79. Toledo M, Munuera J, Salas-Puig X, Santamarina E, Lacuey N, Rovira A. Localisation value of ictal arterial spin-labelled sequences in partial seizures. Epileptic Disord 2011;13(3):336–339.
80. Blauwblomme T, Boddaert N, Chémaly N, et al. Arterial Spin Labeling MRI: a step forward in non-invasive delineation of focal cortical dysplasia in children. Epilepsy Res 2014;108(10):1932–1939.
81. Aronen HJ, Gazit IE, Louis DN, et al. Cerebral blood volume maps of gliomas: comparison with tumor grade and histologic findings. Radiology 1994;191(1):41–51.
82. Knopp EA, Cha S, Johnson G, et al. Glial neoplasms: dynamic contrast-enhanced T2*-weighted MR imaging. Radiology 1999;211(3):791–798.
83. Cha S, Knopp EA, Johnson G, et al. Dynamic contrast-enhanced T2-weighted MR imaging of recurrent malignant gliomas treated with thalidomide and carboplatin. AJNR Am J Neuroradiol 2000;21(5):881–890.
84. Sugahara T, Korogi Y, Kochi M, et al. Correlation of MR imaging-determined cerebral blood volume maps with histologic and angiographic determination of vascularity of gliomas. AJR Am J Roentgenol 1998;171(6):1479–1486.
85. Cha S, Tihan T, Crawford F, et al. Differentiation of low-grade oligodendrogliomas from low-grade astrocytomas by using quantitative blood-volume measurements derived from dynamic susceptibility contrast-enhanced MR imaging. AJNR Am J Neuroradiol 2005;26(2):266–273.
86. Roberts HC, Roberts TP, Bollen AW, Ley S, Brasch RC, Dillon WP. Correlation of microvascular permeability derived from dynamic contrast-enhanced MR imaging with histologic grade and tumor labeling index: a study in human brain tumors. Acad Radiol 2001;8(5):384–391.
87. Patankar TF, Haroon HA, Mills SJ, et al. Is volume transfer coefficient (K(trans)) related to histologic grade in human gliomas? AJNR Am J Neuroradiol 2005;26(10):2455–2465.
88. Grubb RL Jr, Raichle ME, Eichling JO, Ter-Pogossian MM. The effects of changes in PaCO2 on cerebral blood volume, blood flow, and vascular mean transit time. Stroke 1974;5(5):630–639.
89. Warmuth C, Gunther M, Zimmer C. Quantification of blood flow in brain tumors: comparison of arterial spin labeling and dynamic susceptibility-weighted contrast-enhanced MR imaging. Radiology 2003;228(2):523–532.
90. Wolf RL, Wang J, Wang S, et al. Grading of CNS neoplasms using continuous arterial spin labeled perfusion MR imaging at 3 Tesla. J Magn Reson Imaging 2005;22(4):475–482.
91. Järnum H, Steffensen EG, Knutsson L, et al. Perfusion MRI of brain tumours: a comparative study of pseudo-continuous arterial spin labelling and dynamic susceptibility contrast imaging. Neuroradiology 2010;52(4):307–317.
92. Lehmann P, Monet P, de Marco G, et al. A comparative study of perfusion measurement in brain tumours at 3 Tesla MR: arterial spin labeling versus dynamic susceptibility contrast-enhanced MRI. Eur Neurol 2010;64(1):21–26.
93. Qiao XJ, Ellingson BM, Kim HJ, et al. Arterial spin-labeling perfusion MRI stratifies progression-free survival and correlates with epidermal growth factor receptor status in glioblastoma. AJNR Am J Neuroradiol 2015;36(4):672–677.
94. Furtner J, Bender B, Braun C, et al. Prognostic value of blood flow measurements using arterial spin labeling in gliomas. PLoS One 2014;9(6):e99616.
95. De Bazelaire C, Rofsky NM, Duhamel G, Michaelson MD, George D, Alsop DC. Arterial spin labeling blood flow magnetic resonance imaging for the characterization of metastatic renal cell carcinoma(1). Acad Radiol 2005;12(3):347–357.
96. Yamashita K, Yoshiura T, Hiwatashi A, et al. Arterial spin labeling of hemangioblastoma: differentiation from metastatic brain tumors based on quantitative blood flow measurement. Neuroradiology 2012;54(8):809–813.
97. Sugahara T, Korogi Y, Tomiguchi S, et al. Posttherapeutic intraaxial brain tumor: the value of perfusion-sensitive contrast-enhanced MR imaging for differentiating tumor recurrence from nonneoplastic contrast-enhancing tissue. AJNR Am J Neuroradiol 2000;21(5):901–909.
98. Henry RG, Vigneron DB, Fischbein NJ, et al. Comparison of relative cerebral blood volume and proton spectroscopy in patients with treated gliomas. AJNR Am J Neuroradiol 2000;21(2):357–366.
99. Barajas RF Jr, Chang JS, Segal MR, et al. Differentiation of recurrent glioblastoma multiforme from radiation necrosis after external beam radiation therapy with dynamic susceptibility-weighted contrast-enhanced perfusion MR imaging. Radiology 2009;253(2):486–496.
100. Ozsunar Y, Mullins ME, Kwong K, et al. Glioma recurrence versus radiation necrosis? a pilot comparison of arterial spin-

labeled, dynamic susceptibility contrast enhanced MRI, and FDG-PET imaging. Acad Radiol 2010;17(3):282–290.

101. Choi YJ, Kim HS, Jahng GH, Kim SJ, Suh DC. Pseudoprogression in patients with glioblastoma: added value of arterial spin labeling to dynamic susceptibility contrast perfusion MR imaging. Acta Radiol 2013;54(4):448–454.

102. Ho TC, Wu J, Shin DD, et al. Altered cerebral perfusion in executive, affective, and motor networks during adolescent depression. J Am Acad Child Adolesc Psychiatry 2013;52(10):1076–1091.e2.

103. Orosz A, Jann K, Federspiel A, et al. Reduced cerebral blood flow within the default-mode network and within total gray matter in major depression. Brain Connect 2012;2(6):303–310.

104. Raichle ME, MacLeod AM, Snyder AZ, Powers WJ, Gusnard DA, Shulman GL. A default mode of brain function. Proc Natl Acad Sci U S A 2001;98(2):676–682.

105. Barkhof F, Haller S, Rombouts SA. Resting-state functional MR imaging: a new window to the brain. Radiology 2014;272(1):29–49.

106. Duhameau B, Ferré JC, Jannin P, et al. Chronic and treatment-resistant depression: a study using arterial spin labeling perfusion MRI at 3Tesla. Psychiatry Res 2010; 182(2):111–116.

107. Lui S, Parkes LM, Huang X, et al. Depressive disorders: focally altered cerebral perfusion measured with arterial spin-labeling MR imaging. Radiology 2009;251(2):476–484.

108. Colloby SJ, Firbank MJ, He J, et al. Regional cerebral blood flow in late-life depression: arterial spin labelling magnetic resonance study. Br J Psychiatry 2012;200(2):150–155.

109. Pinkham A, Loughead J, Ruparel K, et al. Resting quantitative cerebral blood flow in schizophrenia measured by pulsed arterial spin labeling perfusion MRI. Psychiatry Res 2011;194(1):64–72.

110. Ota M, Ishikawa M, Sato N, et al. Pseudo-continuous arterial spin labeling MRI study of schizophrenic patients. Schizophr Res 2014;154(1-3):113–118.

111. Kindler J, Jann K, Homan P, et al. Static and dynamic characteristics of cerebral blood flow during the resting state in schizophrenia. Schizophr Bull 2015;41:163–170.

112. Schuff N, Zhang Y, Zhan W, et al. Patterns of altered cortical perfusion and diminished subcortical integrity in posttraumatic stress disorder: an MRI study. Neuroimage 2011;54(Suppl 1):S62–S68.

113. Li X, Spence JS, Buhner DM, et al. Hippocampal dysfunction in Gulf War veterans: investigation with ASL perfusion MR imaging and physostigmine challenge. Radiology 2011;261(1):218–225.

114. Grossman EJ, Jensen JH, Babb JS, et al. Cognitive impairment in mild traumatic brain injury: a longitudinal diffusional kurtosis and perfusion imaging study. AJNR Am J Neuroradiol 2013;34(5):951–957, S1–S3.

115. Ge Y, Patel MB, Chen Q, et al. Assessment of thalamic perfusion in patients with mild traumatic brain injury by true FISP arterial spin labelling MR imaging at 3T. Brain Inj 2009;23(7):666–674.

116. Doshi H, Wiseman N, Liu J, et al. Cerebral hemodynamic changes of mild traumatic brain injury at the acute stage. PLoS One 2015;10(2):e0118061. [Published corrections appear in PLoS One 2015;10(5):e0127487 and PLoS One 2015;10(7):e0132750.]

117. Wang Y, West JD, Bailey JN, et al. Decreased cerebral blood flow in chronic pediatric mild TBI: an MRI perfusion study. Dev Neuropsychol 2015;40(1):40–44.

118. Owen DG, Bureau Y, Thomas AW, Prato FS, St Lawrence KS. Quantification of pain-induced changes in cerebral blood flow by perfusion MRI. Pain 2008;136(1-2):85–96.

119. Maleki N, Brawn J, Barmettler G, Borsook D, Becerra l. Pain response measured with arterial spin labeling. NMR Biomed 2013;26(6)664–673.

120. Liu J, Hao Y, Du M, et al. Quantitative cerebral blood flow mapping and functional connectivity of postherpetic neuralgia pain: a perfusion fMRI study. Pain 2013;154(1): 110–118.

121. Kato Y, Araki N, Matsuda H, Ito Y, Suzuki C. Arterial spin-labeled MRI study of migraine attacks treated with rizatriptan. J Headache Pain 2010;11(3):255–258.

122. Pollock JM, Deibler AR, Burdette JH, et al. Migraine associated cerebral hyperperfusion with arterial spin-labeled MR imaging. AJNR Am J Neuroradiol 2008;29(8):1494–1497.

123. Zaharchuk G, Ledden PJ, Kwong KK, Reese TG, Rosen BR, Wald LL. Multislice perfusion and perfusion territory imaging in humans with separate label and image coils. Magn Reson Med 1999;41(6):1093–1098.

124. Hendrikse J, van der Grond J, Lu H, van Zijl PC, Golay X. Flow territory mapping of the cerebral arteries with regional perfusion MRI. Stroke 2004;35(4):882–887.

125. Hendrikse J, Petersen ET, Chng SM, Venketasubramanian N, Golay X. Distribution of cerebral blood flow in the nucleus caudatus, nucleus lentiformis, and thalamus: a study of territorial arterial spin-labeling MR imaging. Radiology 2010;254(3):867–875.

126. Gupta A, Chazen JL, Hartman M, et al. Cerebrovascular reserve and stroke risk in patients with carotid stenosis or occlusion: a systematic review and meta-analysis. Stroke 2012;43(11):2884–2891. [Published correction appears in Stroke 2013;44(10):e137.]

127. Bokkers RP, van Osch MJ, van der Worp HB, de Borst GJ, Mali WP, Hendrikse J. Symptomatic carotid artery stenosis: impairment of cerebral autoregulation measured at the brain tissue level with arterial spin-labeling MR imaging. Radiology 2010;256(1):201–208.

128. Ogawa S, Lee TM, Kay AR, Tank DW. Brain magnetic resonance imaging with contrast dependent on blood oxygenation. Proc Natl Acad Sci U S A 1990;87(24):9868–9872.

129. Villringer A, Dirnagl U. Coupling of brain activity and cerebral blood flow: basis of functional neuroimaging. Cerebrovasc Brain Metab Rev 1995;7(3):240–276.

130. Gauthier CJ, Madjar C, Desjardins-Crépeau L, Bellec P, Bherer L, Hoge RD. Age dependence of hemodynamic response characteristics in human functional magnetic resonance imaging. Neurobiol Aging 2013; 34(5):1469–1485.

131. Tjandra T, Brooks JC, Figueiredo P, Wise R, Matthews PM, Tracey I. Quantitative assessment of the reproducibility of functional activation measured with BOLD and MR perfusion imaging: implications for clinical trial design. Neuroimage 2005;27(2):393–401.